# Petrosal and cranial vascular system of the early Eocene palaeoryctid mammal *Eoryctes melanus* from northwestern Wyoming, USA

JOHN R. WIBLE

Wible, J.R. 2022. Petrosal and cranial vascular system of the early Eocene palaeoryctid mammal *Eoryctes melanus* from northwestern Wyoming, USA. *Acta Palaeontologica Polonica* 67 (1): 203–220.

The petrosal and neighboring bones of the early Eocene palaeoryctid mammal *Eoryctes melanus* are described in tympanic and endocranial views based on CT scan data of the holotype. A second cranium of *E. melanus* has fragments of an osseous bulla, which have been interpreted as possibly formed by an independent entotympanic. The CT scans of the holotype reveal that the medial bullar wall is formed by an expanded rostral tympanic process of the petrosal, but the element(s) in the bullar floor remain unknown. The CT scans also allow for a comprehensive reconstruction of the cranial arterial and venous system. The arterial pattern differs from that in early eutherians by the absence of the arteria diploëtica magna and the bifurcation of the end branches of the stapedial artery dorsal to the tympanic roof. The venous pattern includes a large frontal diploic vein arising from the dorsal sagittal sinus on the midline and running through the frontal bone in a canal. Comparisons are made with other palaeoryctids, various Paleogene mammals (pantolestids, leptictids, apternodontids, apatemyids, and cimolestids) and the extant lipotyphlan *Solenodon paradoxus*. For the last taxon, the structure of the piriform fenestra and associated arteries is detailed. Cranial features support the monophyly of palaeoryctids and suggest possible lipotyphlan affinities.

Key words: Mammalia, Lipotyphla, *Solenodon*, entotympanic, facial nerve, frontal diploic vein, piriform fenestra, stapedial artery, tympanohyal, zygoma.

*John R. Wible [wiblej@carnegiemnh.org; ORCID: https://0000-0002-0721-1228], Section of Mammals, Carnegie Museum of Natural History, 5800 Baum Boulevard, Pittsburgh, Pennsylvania 15206 USA.*

Received 7 June 2021, accepted 19 November 2021, available online 30 March 2022.



## Introduction

The petrosal has long been recognized as an important source for comparisons among mammals, supported by the foundational comparative treatises by the Dutch zoologists Pieter N. van Kampen (1905) and his student Cornelis J. van der Klaauw (1931). While there have been numerous contributions on the topic since, two papers in particular on isolated fossil petrosals, MacIntyre (1972) and Cifelli (1982), influenced me considerably as a graduate student. MacIntyre (1972) described two types of isolated eutherian petrosals (ferungulatan and unguiculatan of Simpson 1945) not found in association with dentitions from the Bug Creek Anthills Quarry of Montana, then considered to be latest Cretaceous (Sloan and Van Valen 1965) but now held to be early Paleocene (Archibald and Lofgren 1990); Cifelli (1982) compared a broad array of isolated petrosals of known Paleogene "condylarths". These papers were groundbreaking in elucidating morphological patterns and offering hypotheses of character polarities for various petrosal features. A third influential paper for me from the same time period, MacPhee (1981), described hard- and soft-tissue structures in late ontogenetic stages of ear regions of some extant primates and "insectivores", emphasizing the importance of development in evaluating the adult condition.

As my contribution to this celebratory volume, I have chosen a topic reminiscent of Cifelli (1982), describing the petrosal of a Paleogene taxon and making relevant comparisons. The choice of taxon has been constrained by specimen availability during museum closures brought on by COVID-19. Fortunately, on MorphoSource.org, I found CT scans of the holotype cranium of *Eoryctes melanus* Thewissen and Gingerich, 1989, a palaeoryctid from the early Eocene of the Clarks Fork Basin, northwestern Wyoming. Thewissen and Gingerich (1989) provided useful descriptions of the outer surfaces of the cranium, including the petrosal. Here, the petrosal is segmented from the cranium, and both its outer

and inner surfaces are described. A reconstruction of certain cranial nerves and vessels is offered as *E. melanus* has some unusual neurovascular features.

Rankin and Holroyd (2014: 919) recently proclaimed that "The Palaeoryctidae are among the most poorly understood groups of early Paleogene, likely insectivorous mammals." This poor understanding includes both membership in and the higher-level relationships of the family. The taxa generally accepted as palaeoryctids (e.g., Gunnell et al. 2008; Rankin and Holroyd 2014) span the Paleocene and early Eocene of western North America, although fossils from other continents have been assigned to the family (e.g., central Asia, Lopatin and Averianov 2004). Regarding the family's higher-level relationships, Palaeoryctidae has been assigned to extant clades, including Soricomorpha (McKenna et al. 1984) and Insectivora (Thewissen and Gingerich 1989), and to extinct clades, such as Deltatheridia (Van Valen 1966) and Proteutheria (Bown and Schankler 1982). There are two recent phylogenetic analyses that include multiple palaeoryctid genera (Halliday et al. 2017, 2019). Both have *Eoryctes* with cimolestids outside of Placentalia and other palaeoryctid genera (i.e., *Palaeoryctes* Matthew, 1913, *Pararyctes* Van Valen, 1966, and *Aaptoryctes* Gingerich, 1982) within Placentalia. Halliday et al. (2019) have these latter three genera as a monophyletic clade, whereas in Halliday et al. (2017) they are paraphyletic in clade including creodonts, palaeanodonts, and pholidotans.

*Institutional abbreviations*.—AMNH, American Museum of Natural History, New York, USA; CM, Carnegie Museum of Natural History, Pittsburgh, USA; MPIH, Neurobiologische Abteilung, Max-Planck-Institut für Hirnforschung, Frankfurt am Main, Germany (collection now housed at AMNH); UM, Museum of Paleontology, University of Michigan, Ann Arbor, USA.

*Other abbreviations*.—1, medial section of caudal tympanic process; 2, lateral section of caudal tympanic process, medial to stapedius fossa; 3, lateral section of caudal tympanic process, lateral to stapedius fossa; asc, alisphenoid canal; bo, basioccipital; bs, basisphenoid; cc, cochlear canalicularis; cd, exposed cochlear duct; cf, cochlear fossula; ci, crista interfenestralis; cin, carotid incisure; cn VII, cranial nerve VII; cp, crista parotica; cpev, capsuloparietal emissary vein; crp, crista petrosa; ef, ethmoidal foramen; egp, entoglenoid process; enav, ethmoidal nerve, artery, and vein; eo, exoccipital; er, epitympanic recess; ew, epitympanic wing; ewas, epitympanic wing of alisphenoid; fdv, frontal diploic vein and its foramen; fi, fossa incudis; fn, facial nerve; fo, foramen ovale; fri, foramen for ramus inferior; frt, foramen for ramus temporalis; fsa, foramen for stapedial artery; gg, geniculate ganglion; gpn, greater petrosal nerve; gri, groove for ramus inferior; grs, groove for ramus superior; hF, hiatus Fallopii; hyf, hypophyseal fossa; iam, internal acoustic meatus; ica, internal carotid artery; icn, internal carotid nerve; ijv, internal jugular vein; iof, infraorbital foramen; ips, inferior petrosal sinus; jf, jugular foramen; lac, lacrimal; lp, lambdoid plate; mcf, middle cranial fossa; npc, nerve of pterygoid canal or its groove; oa, ophthalmic artery; oc, optic canal; on, optic nerve; otc, orbitotemporal canal; otg, orbitotemporal groove; pc, promontory canal; pca, pars canalicularis; pcf, posterior carotid foramen; pco, pars cochlearis; pe, petrosal; pf, piriform fenestra; pr, promontorium; ptp, posttympanic process of squamosal; rcf, rostral cranial fossa; ri, ramus inferior; rio, ramus infraorbitalis; rm, ramus mandibularis; rs, ramus superior; rt, ramus temporalis; rtp, rostral tympanic process; sa, stapedial artery; saf, subarcuate fossa; sc, stapedial canal; sf, stapedius fossa; sips, sulcus for inferior petrosal sinus; smn, stylomastoid notch; so, supraoccipital; sof, sphenorbital fissure; sq, squamosal; sss, sulcus for sigmoid sinus; tc, transverse crest; tcf, transverse canal foramen; th, tympanohyal; tpas, tympanic process of alisphenoid; tt, tegmen tympani; ttf, tensor tympani fossa; $V_2$, maxillary nerve, second division of trigeminal nerve; $V_3$, mandibular nerve, third division of trigeminal nerve; va, vestibular aqueduct.

# Material and methods

The CT scans of the holotype of *Eoryctes melanus*, UM 68074, are on MorphoSource.org Media (https://doi. org/10.17602/M2/M37525) and consist of 1382 tiff files. The scans were done on the Scanco Medical μCT 40, Stony Brook University Center for Biotechnology, Stony Brook University, New York. X, Y, and Z pixel spacing (voxel size) is 0.02 mm. Individual bones of the cranium and neurovascular structures were segmented manually slice by slice using the pencil segmentation tool and measurements were made in Avizo 2019.4 (Thermo Fischer Scientific, Waltham, Massachusetts).

Anatomical terminology follows prior usages by the author (e.g., Wible 1987, 2003, 2008). Soft tissue reconstructions are made based on the author's prior comparative studies (e.g., Wible 1984, 1986, 1987, 2008; Rougier et al. 1992; Rougier and Wible 2006). Neurovascular canals and grooves in the petrosal and braincase walls were segmented in Avizo, producing models from which nerves, arteries, and veins were redrawn on the bone isosurfaces. The extracranial course of the major divisions of the trigeminal nerve and accompanying vessels are based on their foramina of exit and entrance.

# Systematic palaeontology

Mammalia Linnaeus, 1758

Eutheria Gill, 1872

Palaeoryctidae Winge, 1917

Genus *Eoryctes* Thewissen and Gingerich, 1989

*Type species*: *Eoryctes melanus* Thewissen and Gingerich, 1989; see below.

## *Eoryctes melanus* Thewissen and Gingerich, 1989

Figs. 1–6.

1989 *Eoryctes melanus*; Thewissen and Gingerich 1989: 460, figs. 1–7.
2004 *Eoryctes melanus* Thewissen and Gingerich, 1989; Bloch et al. 2004: fig. 15.
2014 *Eoryctes melanus* Thewissen and Gingerich, 1989; Orihuela 2014: fig. 11.

*Material*.—Holotype, UM 68074, CT scans of partial cranium (holotype also includes fragment of dentary, which was not examined); from NW/4, Sec. 1, T55N, R102W, Park County, Clarks Fork Basin, Wyoming, USA (University of Michigan locality SC-133); early Wasatchian Land-Mammal Age, early Eocene.

*Description*.—*Tympanic surface*: In ventral view of UM 68074, the medial aspect of the petrosal contacts the basioccipital anteriorly and exoccipital posteriorly (Fig. 1: pe, bo, eo); as these parts of the occipital are not separated by sutures, a border between them cannot be defined. Given the disposition of the bones and foramina, it seems likely that the jugular foramen (Fig. 1: jf) is between only the exoccipital and petrosal. This is not unusual but the width of the exoccipital puts the jugular foramen in a lateral position, posterior to the pars cochlearis rather than posteromedial to it. The anterior aspect of the petrosal primarily abuts the epitympanic wing of the alisphenoid, but has a narrow contact medially with the basisphenoid and laterally with the squamosal (Fig. 1: ewas, bs, sq); as basi- and alisphenoids are not separated by a suture, their positions are identified as the author has done in extant mammals with the basisphenoid on the central stem of the basicranium and the alisphenoids as the lateral wings (e.g., Wible 2008, 2011). There are narrow gaps between the alisphenoid and petrosal that are not symmetrically arranged between the right and left sides, suggesting that they resulted from breakage and that a piriform fenestra is likely not present. Thewissen and Gingerich (1989: 464) reported a piriform fenestra and "the foramen for the entrance of the internal carotid artery into the braincase" in the sphenoid-petrosal suture. As shown below, the latter is surely not present, but the existence of a narrow piriform fenestra cannot be excluded. The lateral aspect of the petrosal contacts the squamosal (Fig. 1) and the posterior aspect is not covered by other bones and forms the mastoid exposure on the occiput.

There is a foramen in the lateral aspect of the suture between the petrosal and alisphenoid (Fig. 1: fri) that is related to a branch of the stapedial artery described more fully below. A reviewer of an earlier version of this paper, Robert J. Asher, suggested this opening is a piriform fenestra based on a similar opening related to the same branch of the stapedial artery occurring in the extant tenrec *Geogale aurita* Milne Edwards and Grandidier, 1872 (Asher 2001: fig. 6) and the extant lipotyphlan *Solenodon paradoxus* Brandt, 1833 (Wible 2008: fig. 26; Fig. 7B: pf). Following MacPhee (1981), the piriform fenestra is a large, membrane-bound gap in the basicranium anterior to the petrosal that occurs in all fetal mammals; neighboring bones may fill in the membrane to partially or fully close the gap in adults or it may remain open. Being membrane bound, the piriform fenestra is in a common plane; however, the opening for the stapedial artery branch in UM 68074 is in a different plane ventral to that of the remainder of the suture between the alisphenoid and petrosal. This difference in depth is not apparent from the illustration (Fig. 1), but the foramen in question is at the same level as the ventral surface of the promontorium of the left petrosal (Fig. 1: pe). Additionally, the foramen is in an oblique plane, angled anteroventrally, whereas a piriform

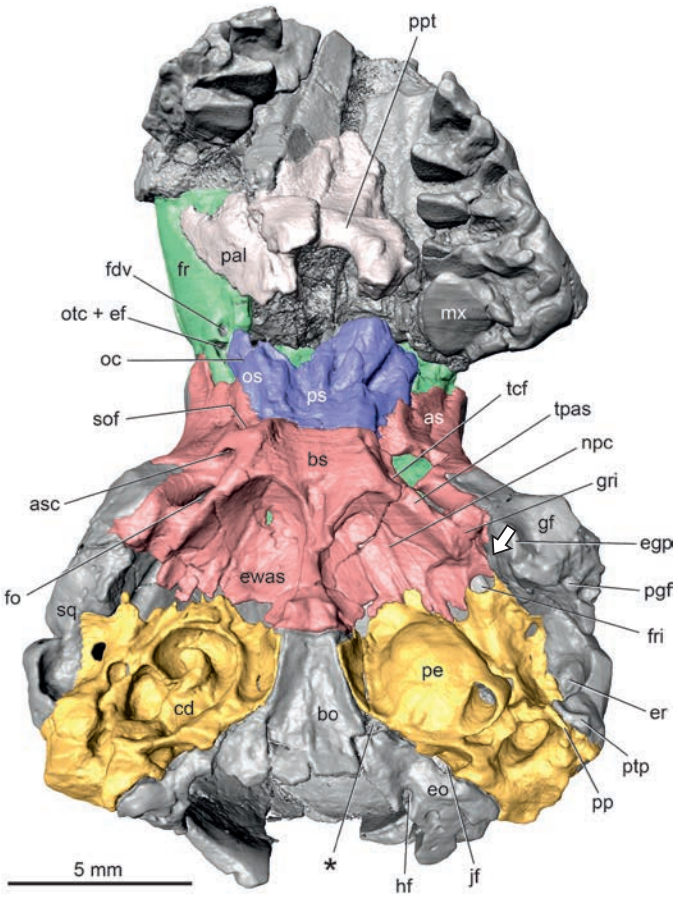


Fig. 1. Palaeoryctid mammal *Eoryctes melanus* Thewissen and Gingerich, 1989, UM 68074 (UM locality SC-133, Clarks Fork Basin, Wyoming, USA; early Wasatchian Land-Mammal Age, early Eocene), isosurface of cranium rendered from CT scans in ventral view. Petrosals in gold; basi- and alisphenoids in red; pre- and orbitosphenoids in blue; frontals in green. Asterisk marks the depression identified as the foramen for the ventral petrosal sinus by Thewissen and Gingerich (1989). Arrow is directed at the Glaserian fissure. Abbreviations: as, alisphenoid; asc, alisphenoid canal; bo, basioccipital; bs, basisphenoid; cd, exposed cochlear duct; egp, entoglenoid process; eo, exoccipital; er, epitympanic recess; ewas, epitympanic wing of alisphenoid; fdv, frontal diploic vein foramen; fo, foramen ovale; fr, frontal; fri, foramen for ramus inferior; gf, glenoid fossa; gri, groove for ramus inferior; hf, hypoglossal foramen; jf, jugular foramen; mx, maxilla; npc, groove for nerve of pterygoid canal; oc, optic canal; os, orbitosphenoid; otc + ef, anterior opening of orbitotemporal canal and ethmoidal foramen; pal, palatine; pe, petrosal; pgf, postglenoid foramen; pp, paroccipital process; ppt, postpalatine torus; ps, presphenoid; ptp, posttympanic process of squamosal; sof, sphenorbital fissure; sq, squamosal; tcf, transverse canal foramen; tpas, tympanic process of alisphenoid.

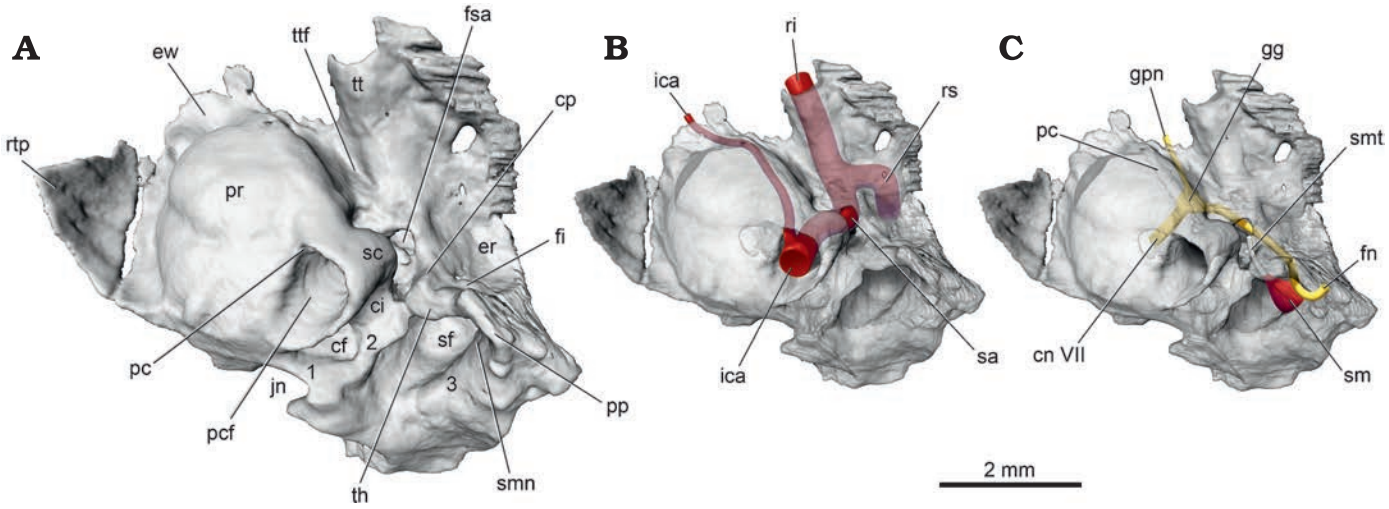


Fig. 2. Palaeoryctid mammal *Eoryctes melanus* Thewissen and Gingerich, 1989, UM 68074 (UM locality SC-133, Clarks Fork Basin, Wyoming, USA; early Wasatchian Land-Mammal Age, early Eocene), isosurface of left petrosal rendered from CT scans in ventral view. **A**. Solid petrosal, medial section of caudal tympanic process (1), lateral section of caudal tympanic process, medial and lateral to stapedius fossa (1, 3, respectively). **B**. Transparent petrosal with internal carotid artery system (in red). **C**. Transparent petrosal with facial nerve (in yellow) and stapedius muscle and its tendon (in red and white, respectively). Neurovascular structures redrawn from Avizo segmentation. Abbreviations: cf, cochlear fossula; ci, crista interfenestralis; cn VII, cranial nerve VII; cp, crista parotica; er, epitympanic recess; ew, epitympanic wing; fi, fossa incudis; fn, facial nerve; fsa, foramen for stapedial artery; gg, geniculate ganglion; gpn, greater petrosal nerve; ica, internal carotid artery; jn, jugular notch; pc, promontory canal; pcf, posterior carotid foramen; pp, paroccipital process; pr, promontorium; ri, ramus inferior; rs, ramus superior; rtp, rostral tympanic process; sc, stapedial canal; sf, stapedius fossa; sm, stapedius muscle; smn, stylomastoid notch; smt, stapedius muscle tendon; th, tympanohyal; tt, tegmen tympani; ttf, tensor tympani fossa.

fenestra is in a horizontal plane. In light of these planar differences, the foramen in question is not equated with the piriform fenestra.

Most of the features of the petrosal are described based on the more completely preserved left element; the right petrosal is damaged, revealing the basal coil of the cochlea (Fig. 1: cd). In a separate section are reconstructions of the major neurovascular structures that leave imprints on the petrosal. For descriptive purposes, the petrosal is divided into the anteroventromedial pars cochlearis for the cochlear duct and saccule and the posterodorsolateral pars canalicularis for the utricle and the semicircular canals.

In ventral view, the pars cochlearis is dominated by the hemispherical promontorium (Fig. 2A: pr). Following the method of Ekdale (2013), the cochlear duct is coiled 720°, equivalent to 2.0 coils. The surface topology of the promontorium reflects these two coils, with a shallow, curved sulcus on the medial aspect marking the separation between the dorsal basal coil and the ventral apical coil. On the posterolateral aspect of the promontorium is a large, round opening, the posterior carotid foramen (Fig. 2A: pcf), leading into two canals of different sizes. The larger lateral canal, the stapedial canal (Fig. 2A: sc), is slightly narrower than the posterior carotid foramen; it bulges dramatically from the promontorial surface and has a short, curved dorsolateral course. The smaller medial canal, the promontory canal (Fig. 2C: pc), is best seen in the transparent petrosal as it produces only a slight bulge from the promontorial surface. The promontory canal is less than half the maximum dimension of the stapedial canal and curves anteromedially across the promontorium. The small posterior opening into the promontory canal is visible just inside the posterior carotid foramen in Fig. 2A.

As is typical in mammals, there are two large windows into the inner ear on the posterior and posterolateral aspects of the promontorium, the fenestra cochleae and fenestra vestibuli, respectively; these are hidden in ventral view. The location of the fenestra cochleae, the round window, is marked by a semilunar depression posterior to it, the cochlear fossula (Fig. 2A: cf). Not visible in the figures is the fenestra vestibuli, the oval window for the footplate of the stapes, situated just dorsal to the terminus of the stapedial canal (Fig. 2A: sc). The fenestra cochleae is oval, wider than tall, with a ratio of mediolateral width to dorsoventral height of 1.8; the margins of the fenestra vestibuli are not as evident but this opening is estimated to have a ratio of length to height minimally of 2.0. The broad column of bone that separates the two windows is the crista interfenestralis (Fig. 2A: ci), which shows a complex morphology in *Eoryctes melanus* discussed with the pars canalicularis below.

A thin shelf arises from the medial and anterior aspects of the promontorium. The anterior component of this continuous shelf is identified as the epitympanic wing and the medial component as the rostral tympanic process (Fig. 2A: ew, rtp). The epitympanic wing is horizontal and meets the epitympanic wing of the alisphenoid to roof the hypotympanic sinus of the alisphenoid; as noted above, there is breakage along the contact between the epitympanic wings of the petrosal and alisphenoid (Fig. 1). Adjacent to the promontorium, the rostral tympanic process is horizontal but farther medially, it curves ventromedially, abutting a concave surface on the lateral aspect of the basioccipital, which represents a tym-

panic process of that bone. A sizeable crack delimits most of the rostral tympanic process from the remainder of the pars cochlearis on both the right and left petrosals (Fig. 1). Thewissen and Gingerich (1989) raised the possibility that this crack might be a suture and that the bone medial to the crack is an independent entotympanic element. However, this is considered unlikely here as the cracks are not entirely symmetrical between the two sides and there is evidence of continuity between the rostral tympanic process and petrosal posterior to the crack on the left side and both anterior and posterior to the crack on the right side. The size of the rostral tympanic process is essentially the same on the left and right sides; however, the comparable structure on the left side of the referred specimen, UM 72623, appears to be slightly more extensive (Thewissen and Gingerich 1989: fig. 4). The right side of UM 72623, has a large, irregular bone fragment ventral to the promontorium and separated from what is identified here as the rostral tympanic process, suggestive that *E. melanus* had at least a partial osseous floor to the tympanic cavity (Thewissen and Gingerich 1989: fig. 4). As noted correctly by Thewissen and Gingerich (1989), it is uncertain whether this bone fragment is part of the petrosal or part of an entotympanic. UM 72623 also preserves fragments of the right ectotympanic, including the ring-shaped posterior crus that widens into a bony plate (Thewissen and Gingerich 1989).

In ventral view, the pars canalicularis is an uneven shelf lateral and posterior to the pars cochlearis. Preserved at the posterolateral corner of this shelf on the left side is a mediolaterally compressed, ventrally directed paroccipital process (Figs. 1, 2A: pp), the mastoid process of some authors (e.g., Butler 1956). The paroccipital process reaches ventrally to the same extent as the promontorium and is covered laterally by the mediolaterally compressed posttympanic process of the squamosal (Fig. 1: ptp). Thewissen and Gingerich (1989) noted that the ventral surface of the mastoid is broken in the holotype but based on the referred specimen reported the absence of a mastoid process. They did identify the structure called a paroccipital process on the left side of the holotype here. Extending anteromedially and decreasing in height from the paroccipital process in UM 68074 is the crista parotica (Fig. 2A: cp); it ends opposite the fenestra vestibuli where it forms the lateral margin of the foramen transmitting the stapedial artery (Fig. 2A: fsa). The medial aspect of the crista parotica has a distinct rounded bulge, which is identified here as the tympanohyal (Fig. 2A: th). Medially, the tympanohyal abuts and is fused to the crista interfenestralis and part of the caudal tympanic process described below (Fig. 2A: 3). Dorsal to this abutment is a conduit connecting the area of the fenestra vestibuli with the rear of the pars canalicularis. Posterior to the tympanohyal and medial to the paroccipital process is a rounded notch, the stylomastoid notch (Fig. 2A: smn) for the facial nerve.

The principal features on the pars canalicularis posterior to the pars cochlearis are the fossa for the stapedius muscle (Fig. 2A: sf) and the caudal tympanic process (Fig. 2A: 1–3). The stapedius fossa is a deep, oval concavity, wider than long, with an area more than four times that of the fenestra vestibuli. The caudal tympanic process, following MacPhee (1981: figs. 2, 50a) and Wible and Shelley (2020: fig. 5), is divided into three sections: (i) medial section; (ii) lateral section, situated medial to the stapedius fossa; and (iii) lateral section, situated lateral to the stapedius fossa. UM 68074 has all three sections: (i) and (ii) are continuous and form a low ridge around the rear of the cochlear fossula; anterolaterally, (ii) merges with the crista interfenestralis and tympanohyal, (iii) remains separate from the other sections and is represented by a low, short ridge medial to the paroccipital process; it contributes to but does not complete a low wall behind the stapedius fossa.

The principal features on the pars canalicularis lateral to the pars cochlearis are the epitympanic recess (Figs. 1, 2A: er) and the tegmen tympani (Fig. 2A: tt). The former makes a roof over the incudomallear articulation and the latter the roof over the middle ear rostral to the epitympanic recess (Klaauw 1931). In UM 68074, the large epitympanic recess is round with its medial half on the petrosal and its lateral half on the squamosal. In the posterior wall of the epitympanic recess is a shallow depression entirely on the petrosal identified as the fossa incudis (Fig. 2A: fi) for the crus breve (short process) of the incus. The tegmen tympani projects anteroventrally from the level of the epitympanic recess and at its anterior extent is roughly even with the ventral promontorial surface. At its widest, the tegmen tympani is just a little narrower than the promontorium. It has a longitudinal prominence marking the course of the stapedial artery and its rostral continuation, the ramus inferior. The anterior margin of the tegmen tympani forms the posterior border of the foramen for the ramus inferior (Fig. 1: fri), which is completed anteriorly by the alisphenoid. Where the tegmen tympani abuts the pars cochlearis is an oval depression, much longer than wide, interpreted as the fossa for the tensor tympani muscle (Fig. 2A: ttf).

*Endocranial surface*: The holotype cranium is sagittally sectioned and the left endocranium is illustrated in Fig. 3A. The petrosal is situated in the posterolateral aspect of the endocranium. Its anterior border, which lies in the middle cranial fossa, is formed by the tegmen tympani in contact with the squamosal and alisphenoid, and the epitympanic wing underlying the alisphenoid. On the petrosal's medial border, the rostral tympanic process has a point contact with the basisphenoid and an extensive one with the basioccipital. The posterior border is formed by the exoccipital ventrally and the supraoccipital dorsally (Fig. 3A: so), but a suture does not distinguish the two. The petrosal's dorsal border is between the pars canalicularis and parietal with a small incursion of squamosal contributing to the groove for the ramus superior (Fig. 3B: grs).

On the petrosal, the pars cochlearis is positioned ventromedially and the pars canalicularis dorsolaterally (Fig. 3B: pco, pca). Each part is dominated by a large opening: the internal acoustic meatus on the former and the subarcuate fossa on the latter (Fig. 3B: iam, saf). Both openings are oval,

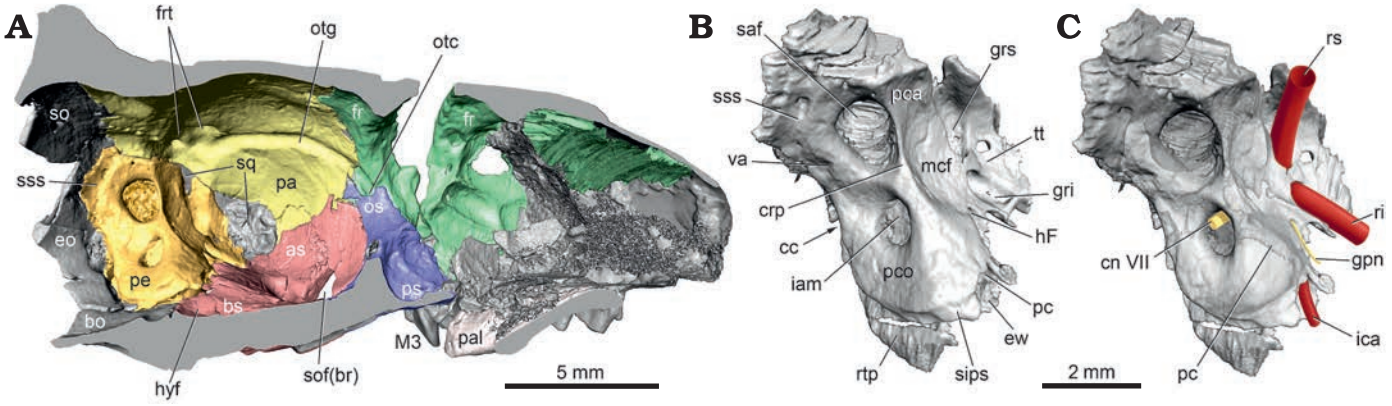


Fig. 3. Palaeoryctid mammal *Eoryctes melanus* Thewissen and Gingerich, 1989, UM 68074 (UM locality SC-133, Clarks Fork Basin, Wyoming, USA; early Wasatchian Land-Mammal Age, early Eocene), isosurfaces rendered from CT scans in medial view. **A**. Left endocranium (petrosal in gold; parietal in yellow; basi- and alisphenoid in red; pre- and orbitosphenoid in blue; frontal in green). **B**. Left petrosal. **C**. Left petrosal with neurovascular structures reconstructed (redrawn from Avizo segmentation; arteries in red; nerves in yellow). Abbreviations: as, alisphenoid; bo, basioccipital; bs, basisphenoid; cc, cochlear canaliculus; cn VII, cranial nerve VII; crp, crista petrosa; eo, exoccipital; ew, epitympanic wing; fr, frontal; frt, foramen for ramus temporalis; gpn, greater petrosal nerve; gri, groove for ramus inferior; grs, groove for ramus superior; hF, hiatus Fallopii; hyf, hypophyseal fossa; iam, internal acoustic meatus; ica, internal carotid artery; M3, upper third molar; mcf, middle cranial fossa; os, orbitosphenoid; otc, orbitotemporal canal; otg, orbitotemporal groove; pa, parietal; pal, palatine; pc, promontory canal; pca, pars canalicularis; pco, pars cochlearis; pe, petrosal; ps, presphenoid; ri, ramus inferior; rs, ramus superior; rtp, rostral tympanic process; saf, subarcuate fossa; sips, sulcus for inferior petrosal sinus; so, supraoccipital; sof(br), sphenorbital fissure (broken); sq, squamosal; sss, sulcus for sigmoid sinus; tt, tegmen tympani; va, vestibular aqueduct.

with the subarcuate fossa more than twice the area of the internal acoustic meatus. Details of the internal acoustic meatus are only preserved on the right petrosal (Fig. 4). It has a shallowly recessed transverse crest (Fig. 4: tc), which delimits the foramen acusticum inferius and superius. The latter has the opening for the facial canal in front and the superior vestibular area behind; the former contains the spiral cribriform tract but additional structures could not be discerned. The subarcuate fossa is wider than deep and its aperture is constricted compared to the fossa proper. Anterior to the subarcuate fossa is a sharp but low crista petrosa (Fig. 3B: crp), which does not extend ventrally onto the pars cochlearis as this area is gently rounded. Anterior to the crista petrosa is a concave area contributing to the posterior wall of the middle cranial fossa (Fig. 3B: mcf), which also represents the roof of the tegmen tympani. In the anteromedial aspect of this concavity is a small opening with a groove emanating from it, the hiatus Fallopii (Fig. 3B: hF). The aperture for the endolymphatic duct, the vestibular aqueduct, is preserved posterior to the subarcuate fossa (Figs. 3B, 4: va), while that for the perilymphatic duct, the cochlear canaliculus, is hidden in the illustrated views (Fig. 3B: cc), deep within the jugular notch, recessed from the tympanic surface.

Several major arteries and veins leave impressions on the endocranial surface of the petrosal. On the dorsal surface of the tegmen tympani are large grooves for the primary branches of the stapedial artery, the ramus superior and ramus inferior (Fig. 3B: grs, gri), the former groove slightly larger than the latter. The anterior (endocranial) opening of the promontory canal (Fig. 3B: pc) is dorsal to the origin of the epitympanic wing. On the ventromedial surface of the pars cochlearis, at the origin of the rostral tympanic process, is a longitudinal sulcus for the inferior petrosal sinus (Fig. 3B: sips). Lastly, posterior to the subarcuate fossa, on the pars canalicularis is the sulcus for the sigmoid sinus (Fig. 3B: sss).

*Reconstructions*.—*Facial nerve*: The facial nerve, cranial nerve VII, courses through the substance of the petrosal in extant mammals (Sisson 1910; Evans 1993; Strandring 2008). Thewissen and Gingerich (1989) noted that the course of the facial nerve in *E. melanus* is not exposed in the middle ear, but is enclosed in a canal. However, they did not provide details of the nerve's course. Boyer and Georgi (2007) stated that the extensive crista parotica in palaeoryctids makes the facial canal appear deeper, but the nerve would still have been in contact with the tympanic cavity, although they did not clarify on what taxon or specimen this was based. The CT scans of UM 68074 help to clarify the facial nerve course as enclosed in canals, with the right petrosal preserving the anterior segment of the course and the left petrosal preserving the posterior segment; this information has been reconstructed onto the left petrosal (Fig. 2C).

The facial nerve enters the dorsal aspect of the internal acoustic meatus (Fig. 3C: cn VII) where it enters the facial canal. After a short ventrolateral course, the facial canal expands into a larger space, the cavum supracochleare, which contains the geniculate ganglion of the facial nerve (Fig. 2C: gg). Two nerves emerge from the geniculate ganglion, the larger is the continuation of the facial nerve and the smaller is the greater petrosal nerve (Fig. 2C: fn, gpn). The latter runs forward in a canal to its exit from the petrosal via the hiatus Fallopii. From there, the greater petrosal nerve leaves the endocranium between the petrosal and alisphenoid, and runs forward in a groove on the epitympanic wing of the alisphenoid (Fig. 1: npc). A second groove is for the internal carotid nerve (Fig. 5: icn), which leaves the endocranium medial to the greater petrosal nerve, to form the nerve of the pterygoid

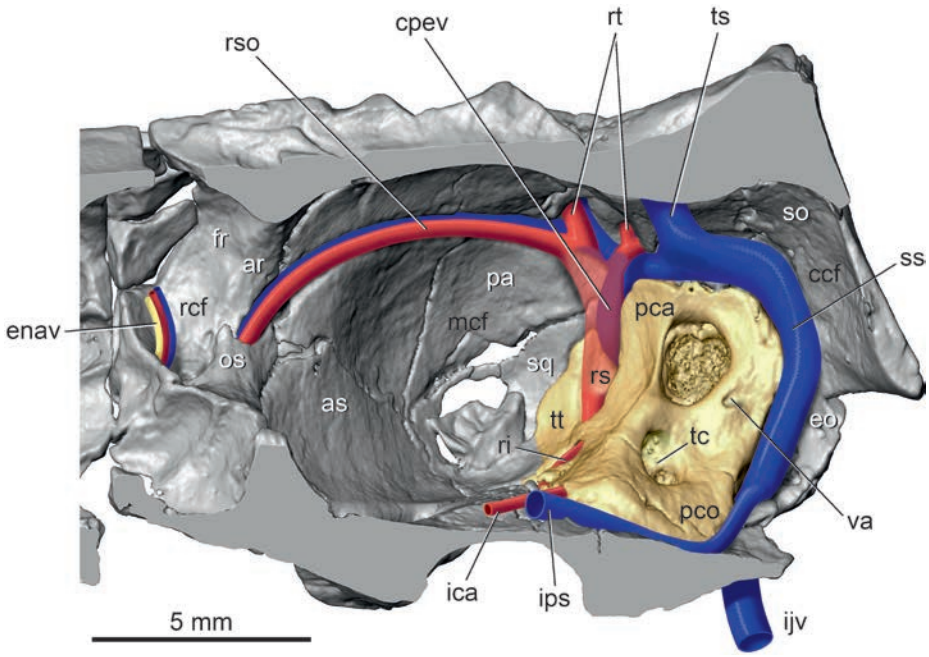


Fig. 4. Palaeoryctid mammal *Eoryctes melanus* Thewissen and Gingerich, 1989, UM 68074 (UM locality SC-133, Clarks Fork Basin, Wyoming, USA; early Wasatchian Land-Mammal Age, early Eocene), isosurface of right endocranium rendered from CT scans in ventral view, with neurovascular structures reconstructed based in part on Avizo segmentation (petrosal in gold; arteries in red; veins in blue; nerves in yellow). Segment of ramus superior is transparent to show hidden capsuloparietal emissary vein; holes in squamosal are damage. Abbreviations: ar, annular ridge; as, alisphenoid; ccf, caudal cranial fossa; cpev, capsuloparietal emissary vein; enav, ethmoidal nerve, artery, and vein; eo, exoccipital; fr, frontal; ica, internal carotid artery; ijv, internal jugular vein; ips, inferior petrosal sinus; mcf, middle cranial fossa; os, orbitosphenoid; pa, parietal; pca, pars canalicularis; pco, pars cochlearis; rcf, rostral cranial fossa; ri, ramus inferior; rs, ramus superior; rso, ramus supraorbitalis with accompanying vein; rt, ramus temporalis with accompanying vein; so, supraoccipital; sq, squamosal; ss, sigmoid sinus; tc, transverse crest; ts, transverse sinus; tt, tegmen tympani; va, vestibular aqueduct.

canal (Fig. 5: npc). The nerve of the pterygoid canal crosses the epitympanic wing of the alisphenoid and enters a short canal in the alisphenoid that opens endocranially.

The larger nerve leaving the geniculate ganglion, the facial nerve, runs posterolaterally in a canal that ultimately opens anterolateral to the stapedius fossa, under cover of the crista parotica and paroccipital process (Fig. 2C). There is a window into this canal opposite the fenestra vestibuli where the stapedial artery enters the canal (Fig. 2A: fsa). The nerve and artery share a short common canal before diverging, with the nerve running posterolaterally and the artery anteriorly (see Fig. 3B, C). After exiting the facial canal near the stapedius fossa, the facial nerve turns ventrally in a shallow groove on the medial aspect of the paroccipital process, posterior to the tympanohyal (Fig. 2C). Its point of exit is the stylomastoid notch (Fig. 2A: smn).

*Cranial vessels*: Thewissen and Gingerich (1989) made a latex endocast from the cranial cavity of UM 68074, which preserved considerable detail about the cranial vascular system. Between the endocast and the grooves, canals, and foramina on the skull exterior, these authors described much of what is reconstructed in the current report, often using different terminology. There are only a few instances where our interpretations differ. Thewissen and Gingerich (1989) did not illustrate the cranial vascular system as is done here to help the reader visualize what is a relatively complex pattern.

The main arteries are reconstructed on the left petrosal of UM 68074 in ventral view in Fig. 2B. It shows a branching pattern in the middle ear similar to that in early eutherians, such as Early Cretaceous *Prokennalestes trofimovi* Kielan-Jaworowska and Dashzeveg, 1989 (Wible et al. 2001), with the internal carotid ("ica" in Fig. 2B) in a transpromontorial position and its primary branch, the stapedial artery, dividing into the ramus superior and ramus inferior (Fig. 2B: sa, rs, ri; see also Fig. 7B). Thewissen and Gingerich (1989) noted correctly that the course of these vessels through the middle ear is shielded by bone, the exception being the stapedial artery as it crosses the fenestra vestibuli. They provided measurements of the bony tubes for the internal carotid prior to the origin of the stapedial artery (approximately 1.0 mm), for the internal carotid after the origin of the stapedial artery in the promontory canal (0.6 mm), and for the stapedial artery (0.8 mm). The CT scans studied here allow measurements of the interior of these bony tubes on the promontorium: the posterior carotid foramen is 0.93 × 0.77 mm (area = 0.71 $mm^2$); the promontory canal is 0.24 × 0.20 mm (area = 0.05 $mm^2$); and the stapedial canal is 0.51 × 0. 49 mm (area = 0.25 $mm^2$). Therefore, the stapedial canal is five times the area of the promontory canal at their origins. The difference in the size of the arteries within their respective canals is even greater given that the promontory canal typically has two occupants, the internal carotid artery and nerve, although there are odd

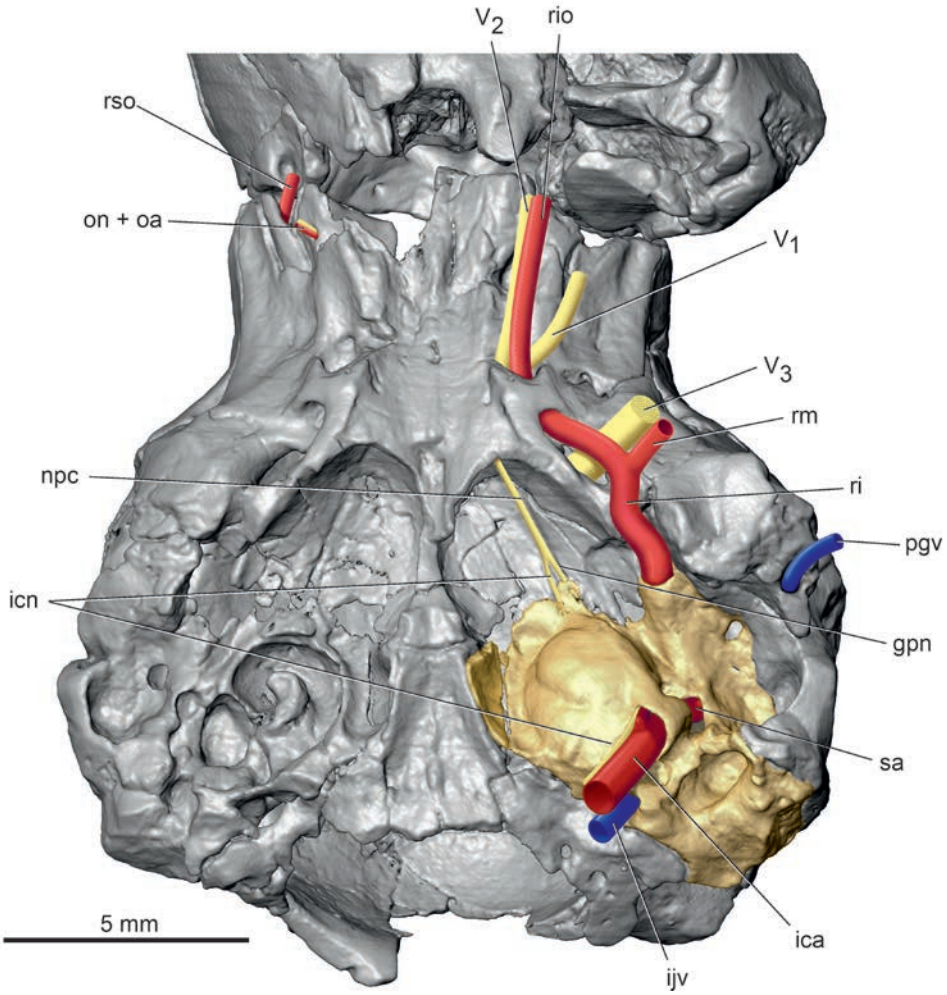


Fig. 5. Palaeoryctid mammal *Eoryctes melanus* Thewissen and Gingerich, 1989, UM 68074 (UM locality SC-133, Clarks Fork Basin, Wyoming, USA; early Wasatchian Land-Mammal Age, early Eocene), isosurface of cranium rendered from CT scans in ventral view, with neurovascular structures reconstructed based in part on Avizo segmentation (left petrosal in gold; arteries in red; veins in blue; nerves in yellow). The alisphenoid canal is broken on the left side in UM 68074 (see Fig. 1), but is reconstructed here to show the course of the ramus infraorbitalis. Abbreviations: gpn, greater petrosal nerve; ica, internal carotid artery; icn, internal carotid nerve; ijv, internal jugular vein; npc, nerve of pterygoid canal; on + oa, optic nerve and ophthalmic artery; pgv, postglenoid vein; ri, ramus inferior; rio, ramus infraorbitalis; rm, ramus mandibularis; rso, ramus supraorbitalis; $V_1$, ophthalmic nerve, first division of trigeminal nerve; $V_2$, maxillary nerve, second division of trigeminal nerve; $V_3$, mandibular nerve, third division of trigeminal nerve.

instances in extant mammals where there is only one occupant, the internal carotid nerve (Conroy and Wible 1978).

The promontory canal opens endocranially at the anterior aspect of the pars cochlearis, dorsal to the epitympanic wing (Fig. 3B). The internal carotid artery curves anteromedially in a faint groove on the dorsal surface of the epitympanic wing (Fig. 3C: ica) and then onto the basisphenoid. Although a carotid groove on the basisphenoid is lacking, the trajectory of the vessel on the petrosal puts the artery wholly lateral to the shallow hypophyseal fossa (Fig. 3A: hyf). Given the relatively small size of the internal carotid artery at the promontory canal, the vertebral artery was likely the most significant contributor of blood to the brain in *E. melanus.*

Beyond the fenestra vestibuli, the stapedial artery enters the foramen (Fig. 2A: fsa) into the common canal for the artery and the facial nerve (see above). The stapedial artery turns anteriorly and divides into its end branches, the ramus superior and ramus inferior (Fig. 3C: rs, ri), which are no longer in a canal but in open grooves on the endocranial surface (Fig. 3B: grs, gri). Thewissen and Gingerich (1989) reported the ramus inferior to be the larger of the two, but they are subequal based on the CT scans.

After traversing the roof of the tegmen tympani, the ramus inferior (Fig. 5) leaves the endocranium at a foramen between the petrosal and alisphenoid (Fig. 1: fri) and runs forward in a groove on the alisphenoid (Fig. 1: gri). Thewissen and Gingerich (1989) identified this groove as the Glaserian fissure, which conducts the chorda tympani and sometimes the ramus inferior from the middle ear in extant mammals (Klaauw 1931). However, a separate Glaserian fissure is identified here for the chorda tympani on the posteromedial surface of the entoglenoid process of the right squamosal in UM 68074 (Fig. 1: arrowhead), a pattern remarkably like that in the extant *Solenodon paradoxus* (Wible 2008). At the foramen ovale (Fig. 1: fo), the ramus inferior divides into the ramus mandibularis and ramus infraorbitalis (Fig. 5: rm,

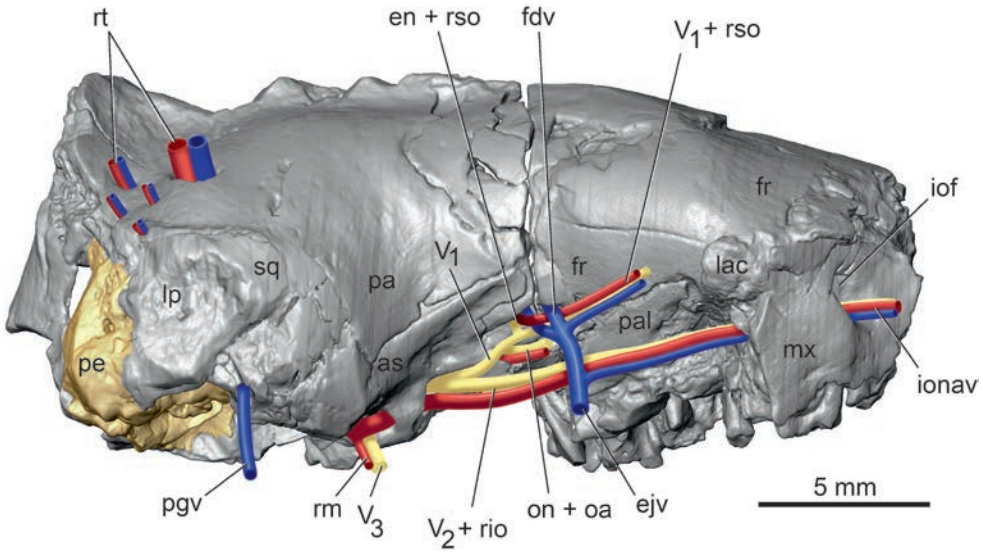


Fig. 6. Palaeoryctid mammal *Eoryctes melanus* Thewissen and Gingerich, 1989, UM 68074 (UM locality SC-133, Clarks Fork Basin, Wyoming, USA; early Wasatchian Land-Mammal Age, early Eocene), isosurface of cranium rendered from CT scans in right lateral view, with neurovascular structures reconstructed based in part on Avizo segmentation (right petrosal in gold; arteries in red; veins in blue; nerves in yellow). As noted in text, the sphenopalatine foramen is not preserved due to damage and, therefore, the expected sphenopalatine artery was omitted from the reconstruction. Abbreviations: as, alisphenoid; ejv, external jugular vein; en + rso, ethmoidal nerve and ramus supraorbitalis with accompanying vein; fdv, frontal diploic vein; fr, frontal; iof, infraorbital foramen; ionav, infraorbital nerve, artery, and vein; lac, lacrimal; lp, lambdoid plate; mx, maxilla; pa, parietal; pal, palatine; pe, petrosal; pgv, postglenoid vein; rm, ramus mandibularis; rt, ramus temporalis with accompanying vein; sq, squamosal; $V_1$ + rso, ophthalmic nerve and ramus supraorbitalis with accompanying vein; $V_2$ + rio, maxillary nerve and ramus infraorbitalis; $V_3$, mandibular nerve.

rio). Reconstruction of the former is based on the prevalent pattern in extant mammals for the origin of the artery accompanying the mandibular nerve, the third division of the trigeminal (Fig. 5: $V_3$), to the lower jaw and of the latter on the presence of the alisphenoid canal (Fig. 1: asc; the alar canal of Thewissen and Gingerich 1989), which transmits the ramus infraorbitalis (= maxillary artery) in extant mammals (e.g., Bugge 1974; Wible 1984, 1987). The alisphenoid canal in UM 68074 conducts the ramus infraorbitalis to the orbit via the sphenorbital fissure (Fig. 1: sof; the rotundo-orbital foramen of Thewissen and Gingerich 1989), which based on the right side of UM 68074 is entirely in the alisphenoid. Within the orbit, the ramus infraorbitalis runs anteriorly with the maxillary nerve, the second division of the trigeminal (Fig. 5: $V_2$), ultimately reaching the infraorbital foramen (Fig. 6: iof) as the infraorbital artery. A major branch of the ramus infraorbitalis in the orbit in extant mammals is the sphenopalatine artery, but as the sphenopalatine foramen was not identifiable in UM 68074 due to damage, I left that artery out of the reconstruction.

From its origin, the ramus superior runs dorsally in a groove on the pars canalicularis and then onto a broader groove on the parietal (Fig. 3). Here, the ramus superior supplies multiple rami temporales (five on the right and three on the left) that exit the endocranium via openings in the parietal (Figs. 4, 6: rt; Fig. 3A: frt). Thewissen and Gingerich (1989) recognized correctly that these foramina transmit arteries and veins, but called them parietal emissary foramina; the term employed here, foramina for rami temporales, is more descriptive of their occupants. On both sides of UM 68074, one foramen for the ramus temporalis is exceedingly large, comparable to the foramen ovale, while the others are considerably smaller. There is no posttemporal canal in UM 68074, which connects the occipital artery and ramus superior via the arteria diploëtica magna in early eutherians (e.g., *Prokennalestes trofimovi*, Wible et al. 2001).

After supplying the rami temporales, the ramus superior curves forward as the ramus supraorbitalis and accompanying vein (Fig. 6: rso) initially in the orbitotemporal groove (sinus canal of Thewissen and Gingerich 1989) on the parietal and then on the frontal (Fig. 3A: otg). The groove leads to a short orbitotemporal canal (Fig. 3A: otc), initially between the frontal and orbitosphenoid and then entirely in the frontal, that, in turn, opens into another short orbitotemporal groove in the floor of the rostral cranial fossa (Fig. 4: rcf). This groove runs to a ventrally directed foramen in the frontal (Fig. 1: otc + ef); a second groove runs dorsolaterally from this foramen on the endocranial sidewall of the rostral cranial fossa. Thewissen and Gingerich (1989) correctly identified this foramen as a combined aperture for the orbitotemporal system (their sinus canal) and ethmoidal foramen, with the ethmoidal nerve, artery, and vein (Fig. 4: enav) occupying the groove running dorsolaterally in the rostral cranial fossa.

One last artery is shown in the reconstructions, the ophthalmic artery accompanying the optic nerve (Fig. 5: oa + on) in the optic canal (Fig. 1: oc). The presence of an ophthalmic artery in the optic canal is conjectural because mammals have two alternative origins for the artery with the optic nerve; it arises intracranially from the circle of Willis (as reconstructed here) or extracranially from the ramus infraorbitalis via the ramus orbitalis (Bugge 1974; Wible 1987) and does not pass through the optic canal.

Regarding the cranial venous system, on the endocast of UM 68074, Thewissen and Gingerich (1989: fig. 7) described a large sinus on the posterior part of the cerebrum and anterior part of the cerebellum that they called the parietal sinus. Their parietal sinus was fed dorsally by the transverse and dorsal (superior) sagittal sinuses and had four primary exits from the cranium: (i) the parietal emissary foramina (= foramina rami temporales); (ii) the sinus canal (= orbitotemporal groove and canal); (iii) the temporal sinus (= the capsuloparietal emissary vein; see Wible 1990) out the retroarticular foramen (= postglenoid foramen); and (iv) the sigmoid sinus out the petro-occipital fissure (= jugular foramen). I agree with their identification of transverse and dorsal sagittal sinuses and the four exits from the parietal sinus, although the first two exits in the reconstruction here are primarily arterial (Figs. 4, 6). However, I question the identification of a parietal sinus by Thewissen and Gingerich (1989). To me, this is an enlargement caused by the juxtaposition of the ramus superior of the stapedial artery internal to the capsuloparietal emissary vein (Fig. 4: cpev) and the veins accompanying the rami temporales and ramus supraorbitalis. Thewissen and Gingerich (1989) observed that the sigmoid sinus is larger than the temporal sinus (= capsuloparietal emissary vein), and I add that the largest foramen for ramus temporalis is also larger than the jugular foramen, both of which are not solely venous in nature.

The endocast of UM 68074 also shows the course of the inferior petrosal sinus (= ventral petrosal sinus of Thewissen and Gingerich 1989: fig. 7), which connects from an area posterolateral to the pons to the sigmoid sinus at the jugular foramen. Despite the connection to the jugular foramen on the endocast, Thewissen and Gingerich (1989: fig. 1) reported that the inferior petrosal sinus left the cranium via a separate foramen located immediately posterior to what is described here as the rostral tympanic process of the petrosal. There is a depression on the left side here (asterisked in Fig. 1), which is preserved differently on the right side. Review of the CT scans reveal that this depression is not a foramen but a blind end. The CT scans also show that the sulcus for the inferior petrosal sinus (Fig. 3B: sips) extends all the way to the jugular foramen as in the endocast. Therefore, the exit point for the inferior petrosal sinus is reconstructed here (Fig. 4: ips) as the jugular foramen where it joins the sigmoid sinus to form the internal jugular vein (Fig. 4: ijv).

During the process of making the endocast of UM 68074, Thewissen and Gingerich (1989) considered the olfactory bulbs to be too delicate and did not include them with the cast. They reconstructed the olfactory bulbs on the endocast (Thewissen and Gingerich 1989: fig. 7) and included a bifurcated vascular structure on the dorsal midline that was labeled "canal for dorsal emissary vein," which was not treated further in their text. These authors did describe the frontal diploic vein, extending from the dorsal midline to the orbit via the foramen caecum (= foramen for frontal diploic vein here; Fig. 1: fdv), which presumably includes their dorsal emissary vein. The CT scans provide additional detail about this vein. The sulcus for the frontal diploic vein arises from the anterior end of the sulcus for the dorsal sagittal sinus on the dorsal midline of the anterior part of the rostral cranial fossa. After a short ventrolateral course, the sulcus enters a canal entirely in the frontal, which it occupies until it emerges in the orbit (Fig. 6: fdv). On the right side, there is a window into the canal where the vein would have been exposed endocranially, whereas on the left side there are two such windows, neither of which corresponds to the window on the right suggesting possible preservational differences. Posterolateral to the main entrance into the canal for the frontal diploic vein is a much smaller foramen on both sides that connects to, and was a distributary of, the main canal. Thewissen and Gingerich (1989: fig. 7) illustrated but did not label this vessel on the endocast.

The CT scans help clarify several other foramina observed by Thewissen and Gingerich (1989). First, they (Thewissen and Gingerich 1989: figs. 1, 2) reported two small venous foramina in the medial wall of the alisphenoid canal (their alar canal) on the left side of UM 68074 that they suggested (Thewissen and Gingerich 1989: 464) "probably carried vessels to the diploic spaces of the basisphenoid". The CT scans show that the posterior of these two foramina (Fig. 1: tcf) opens into a canal passing through the basisphenoid and opening on the opposite side, whereas the anterior foramen is merely a depression. The posterior foramen represents a transverse canal foramen, which carries a vein in extant mammals (Wible 2003, 2008). Second, the endocast of UM 68074 has the impression of a small canal posterior to the optic canal that appears to enter the diploic space of the presphenoid (illustrated but not labeled in Thewissen and Gigerich 1989: fig. 7). The CT scans show that this canal after a short course through the presphenoid joins the more dorsomedially positioned optic canal. In light of its proximity to the sphenorbital fissure and union with the optic canal, a probable occupant of this structure is the ophthalmic vein, although I am not aware of any example of such a separate conduit for this vein in extant mammals. One foramen that the CT scans did not help identify is the small mastoid emissary foramen, which Thewissen and Gingerich (1989) described as piercing the dorsal portion of the mastoid in UM 68074, although absent in UM 72623; I was not able to find this opening in the holotype.

*Stratigraphic and geographic range*.—Type locality and horizon only.

# Discussion

**The entotympanic in *Eoryctes* and other palaeoryctids**.—The composition of the palaeoryctid auditory bulla has been discussed by numerous authors since the description of the first member of the family, *Palaeoryctes puercensis* Matthew, 1913. Because of its relevance in phylogenetic

analyses and the complicated accompanying narrative, the bulla is treated separate from other cranial features here.

In their descriptions of *Eoryctes melanus*, Thewissen and Gingerich (1989) noted that the ventral surface of the auditory bulla was likely ossified based on UM 72623, which preserves much of the fragmentary bullar floor. In reconstructing these fragments, Thewissen and Gingerich (1989) made the fragmentary plate-like ectotympanic the lateral bullar component, but they were undecided about the composition of the medial component, leaving the possibility it might be an independent entotympanic or it might be petrosal in origin, the rostral tympanic process of this report. This ambiguity in composition was followed by Wible et al. (2009) in their taxon-character matrix. However, without comment, Asher et al. (2002) scored the entotympanic present and the ectotympanic a simple ring in *E. melanus* and in *Pararyctes pattersoni* Van Valen, 1966, which is considered by some to be a palaeoryctid (e.g., Gunnell et al. 2008). The latter taxon is known by a skull, UM 80855, but it has not yet been described. In a later study, Silcox et al. (2010) scored *Pararyctes pattersoni* with the entotympanic present, contributing to much of an ossified bulla, and completely covering the moderately expanded ectotympanic, but *E. melanus* was not included in their matrix. However, Silcox et al. (2010: 797) commented on *E. melanus* in their text and stated that it "had a complete, bony auditory bulla, probably formed by the entotympanic, making the ectotympanic aphaneric." This is not the condition reconstructed by Thewissen and Gingerich (1989), who supported a phaneric condition for the ectotympanic and were undecided about whether the major bullar floor element was entotympanic or petrosal.

The oldest palaeoryctid is *Palaeoryctes puercensis* from the early Paleocene of New Mexico. In reporting the holotype and only known specimen at the time, AMNH 15923, Matthew (1913: 310) noted the presence on the left side of part of a "true tympanic ring" (ectotympanic). McDowell (1958) restudied AMNH 15923 and suggested this element was more likely an entotympanic, because of its resemblance to that bone in leptictids; he reported two additional smaller bone fragments in the left ear region, one rod-shaped and the other club-shaped, that he posited might be part of the ectotympanic. In his redescription of AMNH 15923, Van Valen (1966), who also relied on unpublished notes from Bryan Patterson, another vertebrate paleontologist who published extensively on the ear region, came to different conclusions than McDowell on a number of features. Commenting on McDowell's (1958) treatment, Van Valen (1966: 52) stated "At the time he drew the specimen (which is very fragile), it had to be examined through a glass box." Regarding the ring-shaped bone fragment, Van Valen (1966: 53) concluded "I do not know whether the fragment of bulla present is entotympanic, as proposed by McDowell, or tympanic, as claimed by Matthew". Van Valen (1966) also observed that the rod-shaped bone fragment reported by McDowell (1958) was missing and was unsure of the identity of the club-shaped fragment.

A skull of the early Eocene palaeoryctid *Ottoryctes winkleri* Bloch, Secord, and Gingerich, 2004, UM 72624, was reported by Bloch et al. (2004), but with description of the ear region limited to features of the promontorium. For their scores of *O. winkleri*, Silcox et al. (2010) referenced UM 72624 as well as Bloch et al. (2004). They noted the same condition for the entotympanic as they did for *Pararyctes pattersoni*, that is, present, contributing to much of the ossified bulla, and completely covering the moderately expanded ectotympanic. The original report of UM 72624 by Bloch et al. (2004: fig. 9B) included a photograph of the cranium in ventral view. On both sides of the specimen, the promontorium is visible and there do not appear to be any bone fragments that would support the description of a complete ossified bulla formed by the entotympanic and enclosing the ectotympanic, leaving the basis for the scores by Silcox et al. (2010) as uncertain.

This summary highlights the problem of scoring morphology for phylogenetic analysis without descriptive reports or comments supporting the scores. The holotype of *E. melanus*, UM 68074, the subject of the current report, clarifies one issue regarding the composition of the bulla, the identity of the bone appressed to the basioccipital. Thewissen and Gingerich (1989) were uncertain if this was entotympanic or petrosal, but the CT scans reveal continuity with the petrosal, making this the rostral tympanic process (Fig. 2A). The second cranium of *E. melanus*, UM 72623, preserves a bone fragment in the bullar floor of uncertain origin that is in addition to the rostral tympanic process appressed to the basioccipital and the plate-like ectotympanic; this fragment might be an entotympanic or continuous with the rostral tympanic process. Without restudy and description of all the relevant fossils, I treat the composition of the bullar floor and its relationship to the ectotympanic as uncertain in *E. melanus* and other palaeoryctids.

**Comparisons with other palaeoryctids**.—Of the taxa generally accepted as Palaeoryctidae (e.g., Gunnell et al. 2008; Rankin and Holroyd 2014), crania including petrosals have been described, in addition to *Eoryctes melanus*, for *Palaeoryctes puercensis* (Matthew 1913; McDowell 1958; Van Valen 1966) and *Ottoryctes winkleri* (Bloch et al. 2004), and in only one specimen of each. A skull is known for *Pararyctes pattersoni*, UM 80855, which has been scored for the phylogenetic analyses in Asher et al. (2002) and Silcox et al. (2010), but is undescribed.

Only a few features can be evaluated in *Eoryctes*, *Palaeoryctes*, and *Ottoryctes* due to differences in preservation. All have a flat glenoid fossa with an entoglenoid process, large epitympanic recess, round promontorium, and rostral tympanic process that bends ventromedially and contacts the basioccipital. However, in *O. winkleri*, the rostral tympanic process differs in that it extends farther posteriorly and is continuous with the medial aspect of the posterior carotid foramen. An alisphenoid hypotympanic sinus (mesotympanic fossa of Matthew 1913) appears to be present in each,

although it is much smaller in *P. puercensis* and *O. winkleri* than in *E. melanus*. A postglenoid process separate from the entoglenoid process is present in *P. puercensis* and *O. winkleri*, but due to damage the presence of this process cannot be determined for the holotype of *E. melanus*; the drawing of the referred specimen of *E. melanus* in Thewissen and Gingerich (1989: fig. 4) does not provide information for resolving this. All three appear to have the Glaserian fissure separate from the groove for the ramus inferior (Fig. 1; Van Valen 1966; Silcox et al. 2010). An alisphenoid canal, which includes only a posterior opening as the anterior is confluent with the sphenorbital fissure, is present in *E. melanus* and *P. puercensis* (Fig. 1; Van Valen 1966); Silcox et al. (2010) scored an alisphenoid canal as present for *O. winkleri*, but the configuration of the anterior opening was not noted. The alisphenoid canal in *E. melanus* (Fig. 1) differs from *P. puercensis* (Van Valen 1966) in that it is in a common fossa with the foramen ovale; the arrangement in *O. winkleri* is not reported. *Eoryctes melanus* and *O. winkleri* have the tympanic course of the facial nerve enclosed in bone (Fig. 2C; Silcox et al. 2010), whereas it is open in *P. puercensis* (Van Valen 1966).

*Ottoryctes winkleri* resembles *E. melanus* in a number of features that cannot be evaluated in the available publications on *P. puercensis*. Both have vascular foramina in the parietal (Fig. 6; Silcox et al. 2010) and a lambdoid plate (Gawne 1968) on the lateral aspect of the squamosal (Fig. 6: lp), "a shallow oval depression with a rugose texture, bounded by irregular ridges" (Thewissen and Gingerich 1989: 464; Bloch et al. 2004: fig. 9A). Both have a broad, straight contact between the frontal and maxilla on the roof of the rostrum, without maxillary process of the frontal (visible in *E. melanus* in Fig. 6; Bloch et al. 2004: fig. 9A). Both have a small arcuate exposure of the lacrimal on the face (Fig. 6: lac; Bloch et al. 2004: fig. 9A). A postorbital process is lacking (Fig. 6; Bloch et al. 2004: fig. 8) and a transverse canal foramen is present in *E. melanus* and *O. winkleri* (Fig. 1; Silcox et al. 2010). Lastly, the infraorbital foramen opens dorsal to the ultimate premolar (Thewissen and Gingerich 1989; Bloch et al. 2004).

*Ottoryctes winkleri* and *E. melanus* share a feature clearly absent from *P. puercensis*, the presence of bony canals on the promontorium for the internal carotid and stapedial arteries. However, the relative size of these canals differs in the two taxa; whereas the stapedial canal is considerably larger than the promontory canal in *E. melanus* (Fig. 2A), the two appear subequal in *O. winkleri* (Bloch et al. 2004: figs. 9B, 10). Vascular canals are absent in *P. puercensis* (McDowell 1958; Van Valen 1966), but there is controversy about the presence of grooves on the promontorium. McDowell (1958) reported the promontorium to be devoid of vascular grooves, but Van Valen (1966: 55) wrote the internal carotid could "have been on the lateral surface of the promontorium, where matrix covers what may be a groove." Thewissen and Gingerich (1989) stated *P. puercensis* has vascular grooves on the promontorium, whereas Bloch et al. (2004) wrote the promontorium is smooth. Because of the discrepancies, I treat the presence of grooves in *P. puercensis* as unknown, as did Boyer and Georgi (2007) and Silcox et al. (2010).

*Palaeoryctes puercensis* resembles *E. melanus* in several features that cannot be evaluated in *O. winkleri*. Both have a well-developed tympanic process of the alisphenoid (Fig. 1: tpas; pre-otic crest of McDowell 1958) separated from the entoglenoid process of the squamosal (Fig. 1: egp) by the groove for the ramus inferior. Both lack an ectopterygoid process (Fig. 1; Van Valen 1966: pl. 6: 1). The disposition of the three sections of the caudal tympanic process of the petrosal and of the epitympanic wing of the petrosal appears similar in *E. melanus* (Figs. 1, 2A) and *P. puercensis* (Van Valen 1966, pl. 6: 1) as is probably the tensor tympani fossa (Fig. 2A; Van Valen 1966). Differences include the broad basisphenoid in *P. puercensis* (Van Valen 1966: pl. 6: 1) in contrast to the narrow one in *E. melanus* (Fig. 1) and the separation of the tympanohyal from the pars cochlearis in *P. puercensis* (Van Valen 1966), which are in contact in *E. melanus* (Fig. 2A). Regarding the tympanohyal, however, Van Valen (1966) noted that its medial aspect may be broken in *P. puercensis*. Van Valen (1966) reported two openings posterior to the tympanic process of the alisphenoid in *P. puercensis*: a foramen for the internal carotid artery and lateral to it a foramen he labeled a piriform fenestra (his pyriform fenestra in Van Valen 1966: fig. 10), within which he reconstructed the ramus superior of the stapedial artery. Thewissen and Gingerich (1989) noted that the former opening in *E. melanus* likely transmitted the nerve of the pterygoid canal, as reconstructed here (Fig. 5), and posited the same for *P. puercensis*. Regarding the so-called piriform fenestra in *P. puercensis*, the stereophotographs in Van Valen (1966: pl. 6: 1) show a large opening, but it is not possible to evaluate whether it is real from that image alone. However, if it is real, it did not transmit the ramus superior as is it too medial in position for that vessel.

Based on UM 80855, *Pararyctes pattersoni* was scored along with *E. melanus* in the taxon-character matrix in Asher et al. (2002) and along with *O. winkerli* in Silcox et al. (2010), and some features are noted in Boyer and Georgi (2007). As in *E. melanus* and *O. winkleri*, UM 80855 has a rostral tympanic process (Asher et al. 2002; Silcox et al. 2010), vascular foramina in the parietal (Silcox et al. 2010), an alisphenoid canal (Asher et al. 2002; Silcox et al. 2010), and an entoglenoid process (Silcox et al. 2010). Unlike *E. melanus* and *O. winkleri*, UM 80855 has grooves for the internal carotid and stapedial arteries on the promontorium (Silcox et al. 2010), no lambdoid plate (Asher et al. 2002; Silcox et al. 2010), and the infraorbital foramen above M1 (Silcox et al. 2010). Unlike *E. melanus* and *P. puercensis*, UM 80855 has an ectopterygoid process (Silcox et al. 2010), with the condition in *O. winkerli* unknown.

The presence of a jugal and a complete zygomatic arch are features of uncertain distribution among palaeoryctids. In the original description of *P. puercensis*, Matthew (1913) stated the presence or absence of zygomatic arches could not be determined. For *E. melanus*, Thewissen and Gingerich

(1989) reported that the jugal is absent and the zygomatic arch appears to be incomplete. For *O. winkleri*, Bloch et al. (2004) described the zygomatic process of the maxilla as small and the arch as probably incomplete. In scores in matrices, Asher et al. (2002) recorded the arch incomplete in *E. melanus* but complete in *Pararyctes pattersoni*; in contrast, Silcox et al. (2010) had it incomplete with jugal absent in *Pararyctes pattersoni* and *Palaeoryctes* sp. (the cranial character scores of which were based on *P. puercensis*) and either that state or a complete arch in *O. winkleri*. The descriptions and scores do not mesh. The only specimen with published illustrations preserving enough morphology to comment on the presence of the jugal and zygoma is *O. winkleri*. Its zygomatic process of the maxilla (Bloch et al. 2004: fig. 10) is reminiscent of that in *Solenodon paradoxus*, which lacks the jugal and has an incomplete zygoma (McDowell 1958; Wible 2008). If the zygomatic process of *O. winkleri* lacks a facet for the jugal, which cannot be determined from the photographs in Bloch et al. (2004), then that bone should be considered absent and the zygoma incomplete. As to the remaining palaeoryctids, I consider the condition of their zygoma to be unknown.

There is an unnamed taxon of interest to discussions of palaeoryctids that should at least be mentioned, the "Silver Coulee Taxon" of Asher et al. (2002). Wood et al. (2000) reported a late Paleocene *Apternodus*-like form that Asher et al. (2002) included in their treatment of apternodontids. Asher et al. (2002: fig. 51) described and illustrated some details of the basicranium, and scored the two specimens in their taxon-character matrix. In a phylogenetic analysis ordering some characters, the "Silver Coulee Taxon" was sister to *E. melanus*, and *Pararyctes pattersoni* was the outgroup to that pair. Asher et al. (2002) gave the "Silver Coulee Taxon" and *E. melanus* the same scores for the rostral tympanic process, alisphenoid canal, lambdoid plate, and incomplete zygoma; they scored the "Silver Coulee Taxon" the same as *Pararyctes pattersoni* regarding arterial grooves on the promontorium. Hopefully, the crania of this taxon along with that of *Pararyctes pattersoni* will be properly described in the future.

**Comparisons with other Paleogene taxa**.—It is challenging to choose taxa for comparison with Palaeoryctidae given the diversity of opinions regarding their higher-level relationships. Most researchers have focused on other extinct insectivore families, although Halliday et al. (2017, 2019) reported palaeoryctids to be paraphyletic in a clade with with *Eoryctes* falling outside Placentalia and *Palaeoryctes*, *Pararyctes*, and *Aaptoryctes* within Placentalia. Boyer and Georgi (2007) found striking similarities between *Eoryctes melanus* and the pantolestid *Pantolestes longicaudus* Cope, 1872. For comparisons here, I turned to Gunnell et al.'s (2008) chapter on the paraphyletic grouping "Proteutheria." Although not a natural group, it is a reasonable starting place for comparisons in that the included families have at various times been thought to be related. Along with Palaeoryctidae, included in "Proteutheria" by Gunnell et al. (2008) are Cimolestidae, Pantolestidae, and Apatemyidae. Silcox et al. (2010) conducted a phylogenetic analysis that placed apatemyids in Euarchontoglires and aligned palaeoryctids with leptictids. Following this, comparisons here include the "proteutherian" families of Gunnell et al. (2008) plus Leptictidae.

Few cimolestids are known from appropriate material for comparison here, with the most relevant being early Eocene *Didelphodus altidens* (Marsh, 1872), for which the left basicranium is illustrated and described by Van Valen (1966: 43–47, text-fig. 7, pl. 5). The other families are represented by taxa with more complete crania. I use the descriptions and illustrations of early Eocene *Pantolestes longicauda* in Boyer and Georgi (2007) for pantolestids, of early Eocene *Labidolemur kayi* Simpson, 1929, in Silcox et al. (2010) for apatemyids, and of early Oligocene *Leptictis dakotensis* (Leidy, 1868), in Novacek (1986) for leptictids.

Few details are reported or can be gleaned from the illustrations of the basicranium of the cimolestid *Didelphodus altidens* in Van Valen (1966). However, there is little similarity between *D. altidens* and *E. melanus*. The promontorium of the former is flat without rostral tympanic process. It has no vascular canals but appears to have open grooves for a transpromontorial internal carotid and stapedial branch, along with a large piriform fenestra anterior to the promontorium. Like *E. melanus*, *D. altidens* has a flat glenoid fossa with an entoglenoid process as well as an alisphenoid canal with only a posterior opening, the anterior opening being confluent with the sphenorbital fissure. It also appears to have an epitympanic wing and caudal tympanic process arrangement as in *Eoryctes* (Van Valen 1966: pl. 5: 1).

Regarding the pantolestid *Pantolestes longicauda*, Boyer and Georgi (2007: 274) noted it shared the most striking features with *E. melanus* of all the taxa in their comparative set. "These include a frontal that is thickened in the orbitotemporal region, has enlarged frontal diploic veins that communicate with the endocranium through large channels, has a diploic foramen that opens on or near the frontal's contact with the alisphenoid and orbitosphenoid, and has a lamina that extends deep to the parietal posteriorly to the level of the glenoid fossae." They also noted both taxa shared bony canals for the internal carotid and stapedial arteries on the promontorium. In their abstract, Boyer and Georgi (2007) indicated the presence of a rostral tympanic process in *Pantolestes longicauda*, but did not describe it in the text or label it in the figures. The right petrosal appears to have a rostral tympanic process that reaches medially before bending ventrally and abutting the basioccipital (see Boyer and Georgi 2007: fig. 5a, b) as in *E. melanus*; an epitympanic wing also is likely present. Similarities noted here are the broad, straight contact between the frontal and maxilla on the rostrum without a maxillary process of the frontal, small facial exposure of the lacrimal, no postorbital process, parietal longer anteroposteriorly than the frontal on the midline braincase roof, groove for the ramus inferior on the alisphenoid medial to the entoglenoid process, large epitympanic re-

cess, epitympanic wing of the alisphenoid with sulcus for the nerve of the pterygoid canal on it and with a low tympanic process at its anterior end (Boyer and Georgi 2007: fig. 5b: 57), lateral position for the jugular foramen, and absence of a posttemporal foramen as well as of a separate foramen for the inferior petrosal sinus (Boyer and Georgi 2007: figs. 1, 3). Boyer and Georgi (2007: fig. 5a, b) described the tympanohyal in contact with the caudal tympanic process and based on their illustrations this seems similar to the condition in *E. melanus* (Fig. 2A). They noted that *Pantolestes longicauda* appears to have a reduced zygomatic process of the maxilla, as known in *O. winkerli* (Bloch et al. 2004), suggesting the jugal was reduced or absent. Boyer and Georgi (2007) also reported some notable differences between *Pantolestes* and *Eoryctes*: absence of an ossified bulla in *Pantolestes*, bifurcation of the ramus inferior and ramus superior ventral to the tympanic roof in *Pantolestes* versus dorsal in *Eoryctes*, facial nerve in a sulcus in the middle ear, separate foramen rotundum, and foramen for ramus temporalis in the squamosal only in *Pantolestes*. Although Boyer and Georgi (2007) suggested the stapedial bifurcation is ventral to the tympanic roof, they described a remnant of floor for a canal for the ramus inferior in the petrosal, which implies the artery in part ran through the tympanic roof, a possible similarity with *Eoryctes*. *Pantolestes* also does not have a lambdoid plate (Boyer and Georgi 2007: fig. 2a).

Silcox et al. (2010) compared *Labidolemur kayi* with *E. melanus* and found little resemblance between the two. The petrosal of *L. kayi* has an epitympanic wing and rostral tympanic process as in *E. melanus*, but the latter process is quite small and contacts a tympanic process of the basisphenoid (Silcox et al. 2010) whereas the extensive rostral process in *E. melanus* contacts the basioccipital. The arrangement of the caudal tympanic process is similar between the two taxa, but *L. kayi* has a very prominent wall behind the cochlear fossula (Silcox et al. 2010: fig. 4) lacking in *E. melanus* (Fig. 2A). Unlike *E. melanus*, *L. kayi* has unenclosed arteries on the promontorium and an unenclosed facial nerve course (Silcox et al. 2010) as in *P. puercensis*. Both *L. kayi* and *E. melanus* have the posterior opening of the alisphenoid canal in a common fossa with the foramen ovale (Fig. 1; Silcox et al. 2010: fig. 4), but in *L. kayi*, the anterior opening of the alisphenoid canal is separate from the sphenorbital fissure (Silcox et al. 2010) while the two are merged in *E. melanus*. Although *L. kayi* lacks vascular foramina in the parietal, other apatemyids scored by Silcox et al. (2010) have many vascular foramina present as in *E. melanus* (Fig. 6). Similarities noted here include the absence of an ectopterygoid process, absence of a foramen for the inferior petrosal sinus, a lateral position for the jugular foramen, epitympanic wing of the alisphenoid, groove for the ramus inferior on the alisphenoid, absence of the postorbital process, and small facial exposure of the lacrimal. Silcox et al. (2010) stated that an entoglenoid process is lacking in *L. kayi*, but the stereophotographs of the right basicranium (in their fig. 4) appear to show an entoglenoid process continuous with the postglenoid process. Additional differences occurring in *L. kayi* include the origin of the ramus superior and ramus inferior ventral to the tympanic roof, absence of a lambdoid plate, the narrow contact between the frontal and maxilla with a maxillary process of the frontal, and a complete zygoma, formed by well-developed zygomatic processes of the maxilla and squamosal, and the jugal (Silcox et al. 2010).

*Leptictis dakotensis* has an ear region built on a pattern reminiscent of *E. melanus* and *Pantolestes longicauda*. All have a petrosal with an epitympanic wing and a rostral tympanic process that is curved medially, abutting the basioccipital (Novacek 1986: fig. 23), although only in *E. melanus* does this process extend ventral to the basioccipital (Fig. 1). All have a broad epitympanic wing of the alisphenoid that includes a sulcus for the nerve of the pterygoid canal and a low tympanic process at its anterior end (Novacek 1986: figs. 22, 23), although *Leptictis dakotensis* differs in that its tympanic process is continuous laterally with the entoglenoid process and is not separated by a groove for the ramus inferior (Fig. 1). All have a tympanohyal (mastoid tubercle of Novacek 1986) in close proximity to the crista interfenestralis, with fusion in *E. melanus* (Fig. 2A), contact in *Pantolestes longicauda* (Boyer and Georgi 2007), and either full or near contact in *Leptictis dakotensis* (Novacek 1986: figs. 21, 23). *Eoryctes* and *Leptictis* have a similar arrangement for the caudal tympanic process, but this structure is not well preserved in *Pantolestes*. Outside the ear region, all three have a broad contact between the frontal and maxilla on the rostrum (although *Leptictis* has a maxillary process of the frontal (Novacek 1986: fig. 6), a small facial exposure of the lacrimal, no postorbital process, no posttemporal foramen, parietal longer than the frontal on the midline, and an alisphenoid canal (although it has an anterior opening separate from the sphenorbital fissure in *Leptictis*). *Leptictis* differs from *Eoryctes* and *Pantolestes* in having vascular grooves and not canals on the promontorium, a medial position for the jugular foramen, foramen for the frontal diploic vein ("supraorbital foramen" in Novacek 1986: fig. 10) high in the supraorbital margin (far separated from the ethmoidal foramen and the anterior opening of the orbitotemporal canal), well-developed zygomatic process of the maxilla (and complete zygoma with jugal), and an ectopterygoid process. Like *Pantolestes*, *Leptictis* has foramina for rami temporales only in the squamosal and not in the parietal as in *Eoryctes*. *Leptictis* also has a large auditory bulla formed by a separate entotympanic element (Novacek 1986); as noted above, *Eoryctes* has an ossified tympanic floor but the presence or absence of an entotympanic is uncertain. Stereophotographs of the endocranial floor in *Leptictis* (Novacek 1986: fig. 16) reveal the following differences from *Eoryctes*: a well-developed carotid groove on the basisphenoid lateral to the hypophyseal fossa, absence of a well-developed groove for the ramus inferior on the dorsal surface of the tympanic roof, and a more prominent crista petrosa that extends onto the pars cochlearis.

A character complex of uncertain distribution in *Leptictis* concerns the courses of the primary branches of the sta-

pedial artery. Novacek (1980) reconstructed separate exits through the tympanic roof for the ramus superior and ramus inferior, which implied a bifurcation for the stapedial artery within the middle ear; however, he noted (Novacek 1980: 52) that the direct evidence for the ramus inferior course was "somewhat ambiguous". Later, he (Novacek 1986: fig. 26) reconstructed a diminutive ramus inferior originating in the middle ear and exiting lateral to the entoglenoid process. Wible (1987) repeated Novacek's (1980) original characterization for the exit through the tympanic roof, but elsewhere in his paper (Wible 1987: 127) stated that the bifurcation of the stapedial artery in leptictids was dorsal to the tympanic roof, misciting Novacek (1980). MacPhee et al. (1988) characterized the leptictid ramus inferior as large and exiting the middle ear through the tympanic roof, which seems congruent with Novacek's (1980) original reconstruction. Wible's (1987) mistake about the tympanic location of the bifurcation was repeated by Boyer and Georgi (2007). Above, I noted that *Leptictis* lacks the well-developed groove for the ramus inferior on the dorsal surface of the tympanic roof as occurs in *Eoryctes* (Fig. 3B, C). In light of this, I am confident that *Leptictis* does not have an endocranial course for the ramus inferior like *Eoryctes*, but am uncertain which of the tympanic courses for that artery is the correct one or if a ramus inferior is even present in *Leptictis*.

**Comparisons with lipotyphlans**.—In their phylogenetic analysis, Asher et al. (2002) included *Eoryctes* and *Pararyctes* along with various extinct and extant lipotyphlans, and extant tenrecids and macroscelidids. In the trees resulting from their analyses, *Eoryctes* and *Pararyctes* fall within a paraphyletic Lipotyphla that includes afrotherian tenrecids. Only a single cranial character supported that relationship: an alisphenoid canal with an anterior opening confluent with the sphenorbital fissure. In phylogenetic analyses targeting relationships among Cretaceous eutherians, Wible et al.'s (2007, 2009) consensus trees had *E. melanus* as sister taxon to the extant tenrec *Potamogale velox* (Du Chaillu, 1860) in a clade with *Solenodon paradoxus*, supported largely by dental characters. Two subsequent analyses that modified the Wible et al. (2009) taxon-character matrix, Goswami et al. (2011) and Manz et al. (2015), found *Eoryctes* as sister to *Solenodon*. More recently, following Manz et al. (2015), Asher (2018) speculated that *Eoryctes* is a lipotyphlan. Making comparisons with all the taxa considered by these various studies is well beyond the scope of the current report. I limit comparisons here to the extant lipotyphlan *Solenodon paradoxus*, whose skull I have studied elsewhere (Wible 2008), and the apternodontid *Apternodus baladontus* Asher, McKenna, Emry, Tabrum, and Kron, 2002, from the late middle and late Eocene of Montana, treated in Asher et al. (2002).

*Solenodon paradoxus* and *A. baladontus* have ear regions built on a similar pattern, which has differences from that of *E. melanus*. All three have a rostral tympanic process and epitympanic wing, but in *S. paradoxus* (Fig. 7A$_2$) and

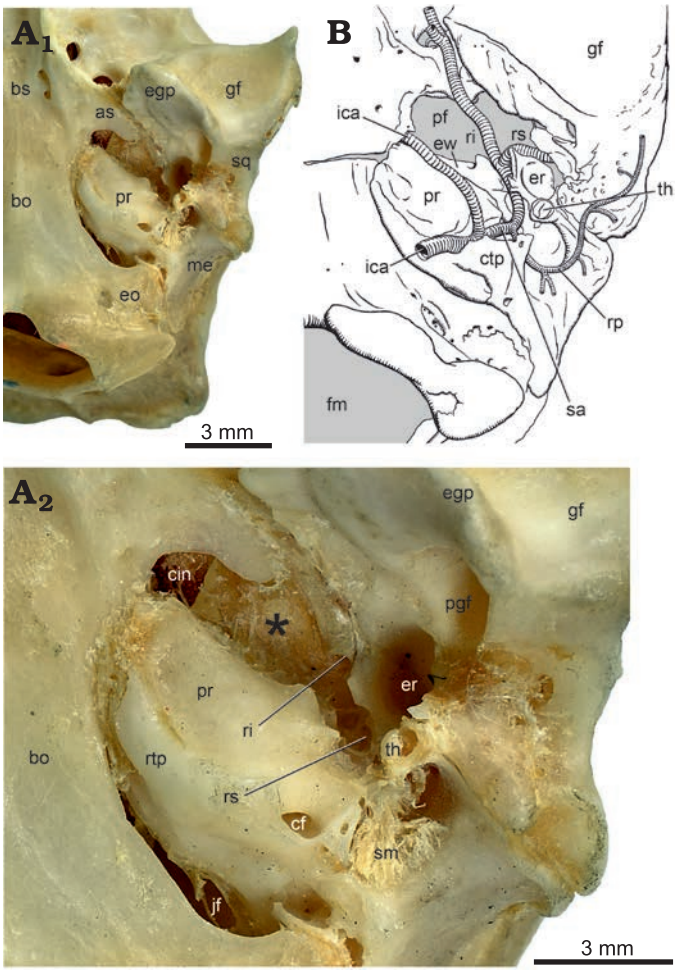


Fig. 7. Lipotyphlan mammal *Solenodon paradoxus* Brandt, 1833, left basicranium in ventral view. **A**. CM 18069, photograph of adult ($A_1$); close-up of ear region ($A_2$). **B**. Drawing of juvenile AMNH 28272 with arterial reconstruction based on MPIH 6863 (modified from Wible 2008: fig. 26C). Caudal tympanic process of the petrosal is broken in CM 18069, exposing the cochlear fossula. Asterisk in $A_2$ is on the membrane of the piriform fenestra in the location of the tensor tympani muscle. Tympanohyal does not contact caudal tympanic process in juvenile AMNH 28272 but does in adults (Wible 2008). Abbreviations: as, alisphenoid; bo, basioccipital; bs, basisphenoid; cf, cochlear fossula; cin, carotid incisure; ctp, caudal tympanic process of petrosal; egp, entoglenoid process; eo, exoccipital; er, epitympanic recess; ew, epitympanic wing of petrosal; fm, foramen magnum; gf, glenoid fossa; ica, internal carotid artery; jf, jugular foramen; me, mastoid exposure; pf, piriform fenestra; pgf, postglenoid foramen; pr, promontorium of petrosal; ri, ramus inferior; rp, ramus posterior; rs, ramus superior; rtp, rostral tympanic process of petrosal; sa, stapedial artery; sm, stapedius muscle; sq, squamosal; th, tympanohyal.

*A. baladontus* (Asher et al. 2002: 29, fig. 11), the rostral tympanic process is a raised ridge recessed laterally from and not in broad contact with the basioccipital. The epitympanic wing in *S. paradoxus* (Fig. 7B) and *A. baladontus* (Asher et al. 2002: 29, fig. 11) is broadly separated from the basi- and alisphenoid by a large piriform fenestra. All three have a similar arrangement to the three sections of the caudal tympanic process, but in *S. paradoxus* (Wible 2008: figs. 25, 26B, 29) and *A. baladontus* (Asher et al. 2002: 29, fig. 11), the medial section is continuous with the

rostral tympanic process and along with the lateral section medial to the stapedius fossa is raised to form a tall wall behind the fenestra cochleae (Fig. 7B). The tympanohyal in all three approximates or contacts the lateral section of the caudal tympanic process (Asher et al. 2002: 26, fig. 11; Wible 2008: fig. 25) and also the crista interfenestralis in *E. melanus*. The arteries within the middle ear follow a similar pattern in all three taxa, but entirely within open grooves or without osseous impressions or petrosal foramina in *S. paradoxus* (Fig. 7) and *A. baladontus*; the facial nerve also runs in an open sulcus in the middle ear in the latter two (Asher et al. 2002: 29, fig. 11; Wible 2008: fig. 27B). The epitympanic recess is more confined in *S. paradoxus* (Fig. 7B) and probably *A. baladontus* (Asher et al. 2002: 26, fig. 11) than in *E. melanus*. All three have an alisphenoid epitympanic wing and tympanic process, but these are very confined in their degree of exposure on the basicranium in *S. paradoxus* (Fig. 7A) and *A. baladontus* (Asher et al. 2002: 26, fig. 11), with the entoglenoid process much larger than the tympanic process of the alisphenoid; *Eoryctes* shows the reverse (Fig. 1). All three have a foramen for the nerve of the pterygoid canal, but it is more medially placed in the lateral aspect of the basisphenoid in *S. paradoxus* (Wible 2008: fig. 27) and *A. baladontus* (Asher et al. 2002: 26, fig. 11). Like *E. melanus*, *S. paradoxus* has a groove for the ramus inferior on the alisphenoid medial to the entoglenoid process and a separate Glaserian fissure on the posteromedial aspect of the entoglenoid (Wible 2008: fig. 26); there is no apparent indication for the course of the ramus inferior in *A. baladontus*.

Outside of the ear region, *S. paradoxus* and *A. baladontus* have a reduced zygomatic process of the maxilla, an incomplete zygoma, and the jugal is absent (Asher et al. 2002; Wible 2008), all of which have been inferred for palaeoryctids (see discussion above). The lacrimal has a tiny facial exposure in *S. paradoxus* (Wible 2008: fig. 2) and it is unclear if a lacrimal is present in *A. baladontus*. A remarkable resemblance between *S. paradoxus* (Wible 2008) and *E. melanus* concerns the frontal diploic vein, which in both is a large vessel communicating across the midline in the roof of the endocranium and occupying a large canal in the frontal. Additionally, their foramen of exit in the orbit is in close proximity to the ethmoidal foramina and anterior opening of the orbitotemporal canal (Wible 2008: fig. 14). For *A. baladontus*, Asher et al. (2002) noted the ethmoidal foramen and anterior opening of the orbitotemporal canal (their sinus canal) are approximated in company with two tiny foramina of unknown function, which I suggest might be for a diminutive frontal diploic vein. *Eoryctes melanus* and *S. paradoxus* (Wible 2008: fig. 21C) have a relatively small endocranial exposure of the squamosal anterior to the petrosal in the middle cranial fossa. A remarkable resemblance between *A. baladontus* (Asher et al. 2002: 28, fig. 11) and *E. melanus* is the presence of a lambdoid plate, which is wholly lacking in *S. paradoxus*. Foramina for the rami temporales are in the parietosquamosal suture and the squamosal in *S. paradoxus* (Wible 2008) and *Apternodus brevirostris* Schlaikjer, 1934 (McDowell 1958: fig. 23A) and not exclusively in the parietal as in *E. melanus*. On the roof of the rostrum, *S. paradoxus* has a well-developed maxillary process of the frontal forming an extensive oblique suture between the frontal and maxilla (Wible 2008: fig. 2) in contrast to the transverse suture in *E. melanus* (Fig. 6). Sutures between the frontal and maxilla are fused in *A. baladontus*, but in *A. brevirostris*, the condition resembles that in *S. paradoxus* (McDowell 1958: fig. 23A). Both *S. paradoxus* (Wible 2008) and *A. baladontus* (Asher et al. 2002) have a large exposure of maxilla in the orbital wall and a tiny exposure of palatine, while the maxilla is excluded from the orbital wall by the prominent palatine in *E. melanus* (Fig. 6).

As reported above, the bifurcation of the ramus superior and ramus inferior of the stapedial artery in *E. melanus* is within the endocranium. Asher (2001) noted the same condition for *S. paradoxus* based on examination of a sectioned juvenile, MPIH 6863, originally included in MacPhee's (1981) ontogenetic study of the tympanic region. Unaware of Asher's (2001) observation, Wible (2008) studying the same sectioned juvenile described the ramus superior entering the cranial cavity via the piriform fenestra (Fig. 7B) with the bifurcation within the middle ear. In the absence of an osseous braincase floor at the piriform fenestra in *S. paradoxus*, how is the plane between structures inside and outside the endocranium defined? As stated above, MacPhee (1981) described the piriform fenestra as a membrane-bound gap occurring in all mammalian embryos, with the membrane providing the plane within which neighboring bones grow to narrow or close the gap. Therefore, it is the membrane of the piriform fenestra that divides the endocranium from extracranial spaces. Figure 7 illustrates the basicranium of an adult *S. paradoxus*, CM 18069, which preserves some soft tissues in situ, including a thick membrane of the piriform fenestra (asterisked in Fig. $7A_2$); the gap in the membrane at the medial corner of the piriform fenestra represents the passageway for the internal carotid artery and nerve into the endocranium (Fig. $7A_2$: cin). Based on study of MPIH 6863, pressed against the ventral (tympanic) surface of the membrane of the piriform fenestra is the tensor tympani muscle (Fig. $7A_2$: in the location of the asterisk). Lateral to the muscle is a membrane-bound canal for the ramus inferior, the posterior opening of which (Fig. $7A_2$: ri) is on the tympanic surface of the membrane of the piriform fenestra. Posterior to this is a small gap in the membrane of the piriform fenestra largely hidden by the squamosal that transports the ramus superior into the endocranium (Fig. $7A_2$: rs). In this adult *S. paradoxus*, the bifurcation of the ramus superior and ramus inferior is within the middle ear as described by McDowell (1958) and Wible (2008). In the section (#1221) of MPIH 6863 illustrated by Asher (2001: fig. 22B), the membrane of the piriform fenestra is the thick connective tissue lying dorsal to the ramus inferior, excluding that artery and the tensor tympani muscle from the endocranium; the endocranial surface of that thick membrane is the dura mater.

# Conclusions

Fox (2004) raised uncertainties about the monophyly of Palaeoryctidae, noting differences in the basicranium and ear region of *Eoryctes* and *Palaeoryctes*, including the degree of closure of the tympanic floor, the size of the middle ear space, and the enclosure of arteries in bony canals in the middle ear. This suggestion was also born out in the phylogenetic analyses of Halliday et al. (2017, 2019) who found *Eoryctes* outside Placentalia and *Palaeoryctes*, *Pararyctes*, and *Aaptoryctes* within Placentalia. The final arbiter of palaeoryctid monophyly is broadscale phylogenetic analysis. However, in lieu of this and despite the differences raised by Fox (2004) and results of Halliday et al. (2017, 2019), the four palaeoryctid genera represented by crania (*Palaeoryctes*, *Pararyctes*, *Eoryctes*, and *Ottoryctes*) share features highly suggestive of shared common ancestry, although the incidence of some characters cannot be determined in all genera because of preservation. All have a rostral tympanic process of the petrosal curved ventromedially in broad contact with the basioccipital, an alisphenoid canal, and an entoglenoid process; *Palaeoryctes*, *Eoryctes*, and *Ottoryctes* have a flat glenoid, an epitympanic wing of the alisphenoid, and the groove for the ramus inferior on the alisphenoid separated from the Glaserian fissure on the squamosal; *Pararyctes*, *Eoryctes*, and *Ottoryctes* have vascular foramina in the parietal for rami temporales; *Eoryctes* and *Ottoryctes* have a transverse canal foramen (and lambdoid plate and intratympanic arterial canals known to be absent in *Palaeoryctes* and *Pararyctes*); and *Eoryctes* and *Palaeoryctes* have a tympanic process of the alisphenoid separated from the entoglenoid process and a similar arrangement of the caudal tympanic process of the petrosal.

The higher-level relationships of palaeoryctids are unsettled as are those for many Paleogene families. Of the taxa compared here palaeoryctids share some unusual resemblances with pantolestids, leptictids, apternodontids, and solenodontids. It seems likely that these all fall in or near the origins of Lipotyphla.

# Acknowledgements

This study was only made possible by access to the CT scans of UM 68074. Doug Boyer (Duke University, Durham, USA) provided access to these data, the collection of which was funded by NSF BCS 1552848. The files were downloaded from www.MorphoSource.org, Duke University. I thank Brian Davis (University of Louisville, USA), Brooke Haiar (University of Lynchburg, USA), and Matt Wedel (Western University of Health Sciences, Pomona, USA) for inviting me to contribute to this volume in honor of my colleague and friend Rich Cifelli (University of Oklahoma, USA). The neurovascular reconstructions in Figs. 2–7 were skillfully completed by Paul Bowden (Carnegie Museum of Natural History, USA). I am grateful for the reviewers, Robert Asher (University of Cambridge, UK) and Maeva Orliac (Université de Montpellier, France), whose comments greatly improved the final version of the contribution. Funding for this project is from National Science Foundation Grant DEB 1654949, the Carnegie Museum of Natural History, and the R.K. Mellon North American Mammal Research Institute.

# References

Archibald, J.D. and Lofgren, D.L. 1990. Mammalian zonation near the Cretaceous–Tertiary boundary. *In*: T.M. Bown and K.D. Rose (eds.), *Dawn of the Age of Mammals in the Northern Part of the Rocky Mountains, North America*, 31–50. Geological Society of America Special Paper 243, Boulder.

Asher, R.J. 2001. Cranial anatomy in tenrecid insectivorans: character evolution across competing phylogenies. *American Museum Novitates* 3352: 1–54.

Asher, R.J. 2018. Diversity and relationships within crown Mammalia. *In*: F. Zachos and R.J. Asher (eds.), *Handbook of Zoology: Mammalian Evolution, Diversity and Systematics*, 301–351. Walter de Gruyter, Berlin.

Asher, R.J., McKenna, M.C., Emry, R.J., Tabrum, A.R., and Kron, D.G. 2002. Morphology and relationships of *Apternodus* and other extinct, zalambdodont, placental mammals. *Bulletin of the American Museum of Natural History* 273: 1–117.

Bloch, J.I., Secord, R., and Gingerich, P.D. 2004. Systematics and phylogeny of late Paleocene and early Eocene Palaeoryctinae (Mammalia, Insectivora) from the Clarks Fork and Bighorn basins, Wyoming. *Contributions from the Museum of Paleontology, The University of Michigan* 31: 119–154.

Bown, T.M. and Schankler, D.M. 1982. A review of the Proteutheria and Insectivora of the Willwood Formation (lower Eocene), Bighorn Basin, Wyoming. *U.S. Geological Survey Bulletin* 1523: 1–79.

Boyer, D.M. and Georgi, J.A. 2007. Cranial morphology of a pantolestid eutherian mammal from the Eocene Bridger Formation, Wyoming, USA: implications for relationships and habitat. *Journal of Mammalian Evolution* 14: 239–280.

Brandt, J.F. 1833. De Solenodonte, novo mammalium insectivorum genere. *Memoires de l'Académie Impériale des Sciences de St. Pétersbourg, Sér. 6, Sciences mathématiques, physiques et naturelles* 2: 459–478.

Bugge, J. 1974. The cephalic arterial system in insectivores, primates, rodents and lagomorphs, with special reference to the systematic classificatjon. *Acta Anatomica* 87 (Supplement 62): 1–160.

Butler, P.M. 1956. The skull of *Ictops* and the classification of the Insectivora. *Proceedings of the Zoological Society of London* 1956: 453–481.

Cifelli, R.L. 1982. The petrosal structure of *Hyopsodus* with respect to that of some other ungulates, and its phylogenetic implications. *Journal of Paleontology* 56: 795–805.

Conroy, G.C. and Wible, J.R. 1978. Middle ear morphology of *Lemur variegatus*: some implications for primate paleontology. *Folia Primatologica* 29: 81–85.

Cope, E.D. 1872. Second account of new Vertebrata from the Bridger Eocene. *Paleontological Bulletin of the American Philosophical Society* 2: 466–468.

Du Chaillu, P.B. 1860. Descriptions of mammals from equatorial Africa. *Proceedings of the Boston Society of Natural History* 7: 358–367.

Ekdale, E.G. 2013. Comparative anatomy of the bony labyrinth (inner ear) of placental mammals. *PLoS ONE* 8 (6): e66624.

Evans, H.E. 1993. *Miller's Anatomy of the Dog.* 1113 pp. W.B. Saunders, Philadelphia.

Fox, R.C. 2004. A new palaeoryctid (Insectivora: Mammalia) from the late Paleocene of Alberta, Canada. *Journal of Paleontology* 78: 612–616.

Gawne, C.E. 1968. The genus *Proterix* (Insectivora, Erinaceidae) of the upper Oligocene of North America. *American Museum Novitates* 2315: 1–26.

Gill, T. 1872. Arrangements of the families of mammals and synoptical table of the characters of the subdivisions of mammals. *Smithsonian Miscellaneous Collections* 11: 1–98.

Gingerich, P.D. 1982. *Aaptoryctes* (Palaeoryctidae) and *Thelysia* (Palaeoryctidae?): new insectivorous mammals from the late Paleocene and early Eocene of western North America. *Contributions from the Museum of Paleontology, University of Michigan* 26: 37–47.

Goswami, A., Prasad, G.V. R., Upchurch, P., Boyer, D.M., Seiffert, E.R., Vermaf, O., Gheerbrant, E., and Flynn, J.J. 2011. A radiation of arboreal basal eutherian mammals beginning in the Late Cretaceous of India. *Proceedings of the National Academy of Science of the United States of America* 108: 16333–16338.

Gunnell, G.F., Bown, T.M., Bloch, J.I., and Boyer, D.M. 2008. "Proteuthe-

ria". *In*: C.M. Janis, G.F. Gunnell, and M.D. Uhen (eds.), *Evolution of Tertiary Mammals of North America, Vol. 2: Small Mammals, Xenarthrans, and Marine Mammals*, 63–81. Cambridge University Press, Cambridge.

Halliday, T.J.D., dos Reis, M., Tamuri, A.U., Ferguson-Gow, H., Yang, Z., and Goswami, A. 2019. Rapid morphological evolution in placental mammals post-dates the origin of the crown group. *Proceedings of the Royal Society B* 286: 20182418.

Halliday, T.J.D., Upchurch, P., and Goswami, A. 2017. Resolving the relationships of Paleocene placental mammals. *Biological Reviews* 92: 521–550.

Kampen, P.N. van 1905. Die Tympanalgegend des Säugetierschädels. *Gegenbaurs Morphologishes Jahrbuch* 34: 321–722.

Kielan-Jaworowska, Z. and Dashzeveg, D. 1989. Eutherian mammals from the Early Cretaceous of Mongolia. *Zoologica Scripta* 18: 347–355.

Klaauw, J.C. van der 1931. The auditory bulla in some fossil mammals with a general introduction to this region of the skull. *Bulletin of the American Museum of Natural History* 62: 1–352.

Leidy, J. 1868, Notice of some remains of extinct Insectivora from Dakota. *Proceedings of the Academy of Natural Sciences of Philadelphia* 1868: 315–316.

Linnaeus, C. 1758. *Systema naturæ per regna tria naturæ, secundum classes, ordines, genera, species, cum characteribus, differentiis, synonymis, locis. Tomus I. Editio decima, reformata*. 824 pp. Laurentius Salvius, Stockholm.

Lopatin, A.V. and Averianov, A.O. 2004. New Palaeoryctidae (Mammalia) from the Eocene of Kyrgyzstan and Mongolia. *Paleontological Journal* 38: 556–562.

MacIntyre, G.T. 1972. The trisulcate petrosal pattern of mammals. *In*: T. Dobzhansky, M.K. Hecht, and W.C. Steere (eds.), *Evolutionary Biology, Vol. 6*, 275–303. Appleton-Century-Crofts, New York.

MacPhee, R.D.E. 1981. Auditory region of primates and eutherian insectivores: morphology, ontogeny, and character analysis. *Contributions to Primatology* 18: i–xvi, 1–282.

MacPhee, R.D.E., Novacek, M.J., and Storch, G. 1988. Basicranial morphology of early Tertiary erinaceomorphs and the origin of primates. *American Museum Novitates* 2921: 1–42.

Manz, C.L., Chester, S.G.B., Bloch, J.I., Silcox, M.T. and Sargis, E.J. 2015. New partial skeletons of Palaeocene Nyctitheriidae and evaluation of proposed euarchontan affinities. *Biology Letters* 11: 20140911.

Marsh, O.C. 1872. Preliminary description of new Tertiary mammals. *American Journal of Science*, *Series 3* 4: 122–128, 202–224.

Matthew, W.D. 1913. A zalambdodont insectivore from the basal Eocene. *Bulletin of the American Museum of Natural History* 32: 307–314.

McDowell, S.B., Jr. 1958. The Greater Antillean insectivores. *Bulletin of the American Museum of Natural History* 115: 113–214.

McKenna, M.C., Xue, X., and Zhou, M. 1984. *Prosarcodon lonanensis*, a new Paleocene rnicropternodontid palaeoryctoid insectivore from Asia. *American Museum Novitates* 2780: 1–17.

Milne Edwards, A. and Grandidier, A. 1872. Description d'un nouveau mammifère insectivore de Madagascar (*Geogale aurita*). *Annales des Sciences Naturelles, Zoologie et Paléontologie* 15 (19): 1–5.

Novacek, M.J. 1980. Cranioskeletal features in tupaiids and selected Eutheria as phylogenetic evidence. *In*: W.P. Luckett (ed.), *Comparative Biology and Evolutionary Relationships of Tree Shrews*, 35–93. Plenum Press, New York.

Novacek, M.J. 1986. The skull of leptictid insectivorans and higher classification of eutherian mammals. *Bulletin of the American Museum of Natural History* 183: 1–111.

Orihuela, J. 2014. Endocranial morphology of the extinct Antillean shrew *Nesophontes* (Lipotyphla: Nesophontidae) from natural and digital endocasts of Cuban taxa. *Palaeontologia Electronica* 17.2.22A: 1–12.

Rankin, B.D. and Holroyd, P.A. 2014. *Aceroryctes dulcis*, a new palaeoryctid (Mammalia, Eutheria) from the early Eocene of the Wasatch Formation of southwestern Wyoming, USA. *Canadian Journal of Earth Sciences* 51: 919–926.

Rougier, G.W. and Wible, J.R. 2006. Major changes in the mammalian ear region and basicranium. *In*: M.T. Carrano, T.J. Gaudin, R.W. Blob, and J.R. Wible (eds.), *Amniote Paleobiology: Perspectives on the Evolution of Mammals, Birds, and Reptiles*, 269–311. University of Chicago Press, Chicago.

Rougier, G.W., Wible, J.R., and Hopson, J.A. 1992. Reconstruction of the cranial vessels in the Early Cretaceous mammal *Vincelestes neuquenianus*: implications for the evolution of the mammalian cranial vascular system. *Journal of Vertebrate Paleontology* 12: 188–216.

Schlaikjer, E.M. 1934. A new fossil zalambdodont insectivore. *American Museum Novitates* 698: 1–8.

Silcox, M.T., Bloch, J.I., Boyer D.M., and Houde, P. 2010. Cranial anatomy of Paleocene and Eocene *Labidolemur kayi* (Mammalia: Apatotheria), and the relationships of Apatemyidae to other mammals. *Zoological Journal of the Linnean Society* 160: 773–825.

Simpson, G.G. 1929. A collection of Paleocene mammals from Bear Creek, Montana. *Annals of Carnegie Museum* 19 (6): 115–122.

Simpson, G.G. 1945. The principles of classification and a classification of mammals. *Bulletin of the American Museum of Natural History* 85: 1–350.

Sisson, S. 1910. *A Text-book of Veterinary Anatomy.* 826 pp. W.B. Saunders Company, Philadelphia.

Sloan, R.E. and Van Valen, L. 1965. Cretaceous mammals from Montana. *Science* 148: 220–227.

Strandring, S. (ed.). 2008. *Gray's Anatomy. 40th Edition*. 1551 pp. Churchill, Livingstone.

Thewissen, J.G.M. and Gingerich, P.D. 1989. Skull and endocranial cast of *Eoryctes melanus*, a new palaeoryctid (Mammalia: Insectivora) from the early Eocene of western North America. *Journal of Vertebrate Paleontology* 9: 459–470.

Van Valen, L. 1966. Deltatheridia, a new order of mammals. *Bulletin of the American Museum of Natural History* 132: 1–126.

Wible, J.R. 1984. *The Ontogeny and Phylogeny of the Mammalian Cranial Arterial Pattern*. 705 pp. Ph.D. Dissertation, Duke University, Durham.

Wible, J.R. 1986. Transformations in the extracranial course of the internal carotid artery in mammalian phylogeny. *Journal of Vertebrate Paleontology* 6: 313–325.

Wible, J.R. 1987. The eutherian stapedial artery: character analysis and implications for superordinal relationships. *Zoological Journal of the Linnean Society* 91: 107–135.

Wible, J.R. 2003. On the cranial osteology of the short-tailed opossum *Monodelphis brevicaudata* (Didelphidae, Marsupialia). *Annals of Carnegie Museum* 72: 137–202.

Wible, J.R. 2008. On the cranial osteology of the Hispaniolan solenodon, *Solenodon paradoxus* Brandt, 1833 (Mammalia, Lipotyphla, Solenodontidae). *Annals of Carnegie Museum* 77: 321–402.

Wible, J.R. 2009. The ear region of the pen-tailed treeshrew, *Ptilocercus lowii* Gray, 1848 (Placentalia, Scandentia, Ptilocercidae). *Journal of Mammalian Evolution* 16: 199–234.

Wible, J.R. 2011. On the treeshrew skull (Mammalia, Placentalia, Scandentia). *Annals of Carnegie Museum* 79: 149–230.

Wible, J.R. and Shelley, S.L. 2020. Anatomy of the petrosal and middle ear of the brown rat, *Rattus norvegicus* (Berkenhout, 1769) (Rodentia, Muridae). *Annals of Carnegie Museum* 86: 1–35.

Wible, J.R., Rougier, G.W., Novacek, M.J., and Asher, R.J. 2007. Cretaceous eutherians and Laurasian origin for placental mammals near the K-T boundary. *Nature* 47: 1003–1006.

Wible, J.R., Rougier, G.W., Novacek M.J., and Asher, R.J. 2009. The eutherian mammal *Maelestes gobiensis* from the Late Cretaceous of Mongolia and the phylogeny of Cretaceous Eutheria. *Bulletin of the American Museum of Natural History* 327: 1–123.

Wible, J.R., Rougier, G.W., Novacek, M.J., and McKenna, M.C. 2001. Earliest eutherian ear region: a petrosal referred to *Prokennalestes* from the Early Cretaceous of Mongolia. *American Museum Novitates* 3322: 1–44.

Winge, H. 1917. Udsigt over Insektaedernes indbyrdes Slaegtskab. *Videnskabelige Meddelelser fra Dansk Naturhistorisk Forening Copenhagen* 68: 83–203.

Wood, C.B., McKenna, M.C., and Bosko, D. 2000. An old specimen of a new undescribed late Paleocene *Apternodus*-like insectivore. *Journal of Vertebrate Paleontology* 20 (Supplement to 3): 80A.